THE GEOLOGICAL SOCIETY OF AMERICA®

Structural modeling of the Western Transverse Ranges: An imbricated thrust ramp architecture

Y. Levy[1,2], T.K. Rockwell[1], J.H. Shaw[3], A. Plesch[3], N.W. Driscoll[2], and H. Perea[2,4]

[1]DEPARTMENT OF GEOLOGICAL SCIENCES, SAN DIEGO STATE UNIVERSITY, 5500 CAMPANILE DRIVE, SAN DIEGO, CALIFORNIA 92182, USA
[2]SCRIPPS INSTITUTION OF OCEANOGRAPHY, UNIVERSITY OF CALIFORNIA–SAN DIEGO, 9500 GILMAN DRIVE, LA JOLLA, CALIFORNIA 92037, USA
[3]DEPARTMENT OF EARTH AND PLANETARY SCIENCES, HARVARD UNIVERSITY, 20 OXFORD STREET, CAMBRIDGE, MASSACHUSETTS 02138, USA
[4]INSTITUT DE CIENCIES DEL MAR, CONSEJO SUPERIOR DE INVESTIGACIONES CIENTIFICAS, PASSEIG MARITIM DE LA BARCELONETA, 37-49, 08003 BARCELONA, SPAIN

ABSTRACT

Active fold-and-thrust belts can potentially accommodate large-magnitude earthquakes, so understanding the structure in such regions has both societal and scientific importance. Recent studies have provided evidence for large earthquakes in the Western Transverse Ranges of California, USA. However, the diverse set of conflicting structural models for this region highlights the lack of understanding of the subsurface geometry of faults. A more robust structural model is required to assess the seismic hazard of the Western Transverse Ranges. Toward this goal, we developed a forward structural model using Trishear in MOVE® to match the first-order structure of the Western Transverse Ranges, as inferred from surface geology, subsurface well control, and seismic stratigraphy. We incorporated the full range of geologic observations, including vertical motions from uplifted fluvial and marine terraces, as constraints on our kinematic forward modeling. Using fault-related folding methods, we predicted the geometry and sense of slip of the major faults at depth, and we used these structures to model the evolution of the Western Transverse Ranges since the late Pliocene. The model predictions are in good agreement with the observed geology. Our results suggest that the Western Transverse Ranges comprises a southward-verging imbricate thrust system, with the dominant faults dipping as a ramp to the north and steepening as they shoal from ~16°–30° at depth to ~45°–60° near the surface. We estimate ~21 km of total shortening since the Pliocene in the eastern part of the region, and a decrease of total shortening west of Santa Barbara down to 7 km near Point Conception. The potential surface area of the inferred deep thrust ramp is up to 6000 km^2, which is of sufficient size to host the large earthquakes inferred from paleoseismic studies in this region.

LITHOSPHERE; v. 11; no. 6; p. 868–883 | Published online 4 November 2019 https://doi.org/10.1130/L1124.1

INTRODUCTION

Active fold-and-thrust belts produce destructive earthquakes, such as the M 7.9 Wenchuan earthquake in 2008 and the M 7.3 Gorkha earthquake in 2015 (Hayes et al., 2016). Estimating the geometry of faults at depth is important for risk assessment because the deep connectivity in thin-skinned fold-and-thrust belts determines the plausible sizes of earthquakes that a system can host (Wells and Coppersmith, 1994). Furthermore, many structural predictive models have been developed because this class of structures acts as potential hydrocarbon traps (e.g., Suppe, 1983; Suppe and Medwedeff, 1990; Erslev, 1991; Groshong, 1994; Poblet and McClay, 1996). The Western Transverse Ranges (Fig. 1) of southern California is an active fold-and-thrust belt (Namson and Davis, 1988; Shaw and Suppe, 1994) in a highly populated region, with 18 million people inhabiting the Los Angeles Basin along its southern margin. Recent studies of coastal uplift and borehole transects across a fold scarp have revealed that very large and rapid uplift events have occurred along the Pitas Point/Ventura fault system (Fig. 1B, localities a and b; Hubbard et al., 2014), the offshore part of which is referred to as the Pitas Point fault and the onshore part of which is referred to as the Ventura fault. The observed uplift events were estimated to be the result of Mw 7.5–8 earthquakes (Rockwell et al., 2016; McAuliffe et al., 2015). For instance, Holocene coastal marine terraces near Punta Gorda between Ventura and Santa Barbara, California, record four uplift events in the past 6.7 k.y., with an average of 10 m per uplift event (Rockwell et al., 2016), Punta Gorda (Fig. 1B, locality a) is situated on the axis of the Pitas Point/Ventura Avenue anticline along a section where the Pitas Point fault is mostly or completely blind, so much or all of the fault slip is translated into uplift through folding and back-thrusting. Similarly, the onshore Ventura fault has produced up to 6 m of vertical deformation per event (McAuliffe et al., 2015). These uplift events are comparable to the magnitude of uplift observed in the 1999 M 7.6 Chi-Chi earthquake in Taiwan (Ma et al., 1999), and scaling relations (Wells and Coppersmith, 1994) suggest that these are the result of large earthquakes. Considering the complex structural geology in the upper several kilometers of the Western Transverse Ranges, the observed uplifts were suggested to be the result of multisegment thrust fault ruptures (Hubbard et al., 2014). However, this explanation has been questioned based on arguments of fault complexity (Sorlien and Nicholson, 2015).

Various structural models (e.g., Yeats et al., 1988; Namson and Davis, 1988; Shaw and Suppe, 1994; Hubbard et al., 2014; Sorlien and Nicholson, 2015) have been advanced over the years to describe the complex fault architecture in the Western Transverse Ranges. Nevertheless, there are ongoing debates regarding these proposed models, mainly centered on the direction of dip of the primary structures and their senses of slip. As a result, series of competing, alternative models for these structures are represented

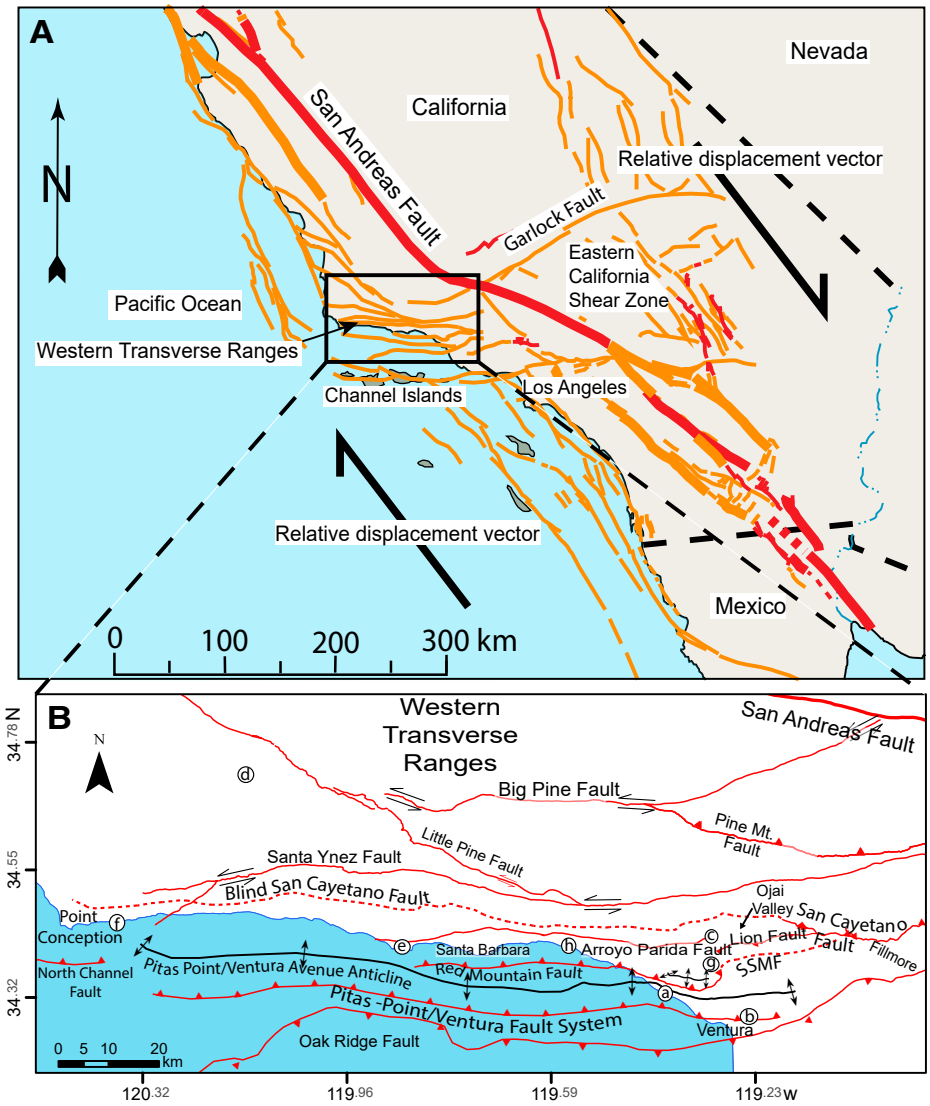

Figure 1. (A) Regional fault map of California. The relative motion of the Pacific and North American plates is right lateral and is on the order of 45 mm/yr. The Western Transverse Ranges, located within the black box located south of the Big Bend of the San Andreas fault, accommodate the shortening resulting from the geometry of the Big Bend of the San Andreas fault and the right-lateral strike-slip faults southeast of the channel islands. (B) Main faults in the Western Transverse Ranges and location of geomorphic studies in the region: a (Punta Gorda)—uplifted and tilted marine terraces (Rockwell et al., 2016), b—location of the sections from McAuliffe et al. (2015), c—uplifted fluvial terraces with no tilting (Rockwell et al., 1984), d—uplifted fluvial terraces with some tilting (Farris, 2017), e—marine oxygen isotope stage (MIS) 3 marine terraces demonstrating an uplift rate of ~1 mm/yr at Isla Vista (Gurrola et al., 2014), f—MIS 5 marine terraces demonstrating an uplift rate of at least 0.3 mm/yr between Gaviota and Point Conception (Rockwell et al., 1992), g—tilted and uplifted fluvial terraces with no horizontal deflection (Rockwell et al., 1984, 1988), h—Carpenteria. SSMF—South Sulphur Mountain fault.

in the Southern California Earthquake Center's (SCEC) Community Fault Model (CFM; Nicholson et al., 2017; Plesch et al., 2007) and used in regional hazards assessments.

In this work, we incorporated published geological observations, including late Quaternary geologic vertical motions, to be used as interpretive constraints on a kinematic forward model for the Western Transverse Ranges. We started with the detailed regional mapping by Dibblee (2002) and incorporated subsurface data from the numerous oil wells in the region, as well as offshore seismic reflection profiles and their interpretations (Sorlien and Nicholson, 2015) and published geological observations (Davis and Namson, 1998; Hubbard et al., 2014; Jackson, 1981; Namson and Davis, 1988; Sarna-Wojcicki and Yerkes, 1982; Schlueter, 1976; Yeats, 1983). From these sources, we constructed seven geologic cross sections of the upper few kilometers, with sections across the eastern Ventura Basin westward to near Point Conception (Fig. 2). We then applied forward modeling using the Trishear module in Move® (https://www.mve.com/) to replicate or match the primary structural elements of the Western Transverse Ranges, as shown in the geologic cross section, with the intent of developing a crustal-scale model of the entire seismogenic portion of the crust. Incorporated into this modeling was information on the local and regional vertical motions, which aided in constraining the fault dip at depth. The final result is a retrodeformable, area-balanced kinematic model that matches and accounts for the surficial and shallow subsurface geology, the local and regional structural relief, and late Quaternary vertical motions as determined from geologic studies of uplifted and deformed marine and fluvial terrace sequences. We applied this model to test the possibility that the Western Transverse Ranges hosts a fault system that may be capable of generating earthquakes responsible for the large uplift events observed in the region.

GEOLOGICAL BACKGROUND

The Western Transverse Ranges are composed of continental plutonic and metamorphic basement in the east and juxtaposed or accreted oceanic ophiolitic–Franciscan basement complex in the west, both overlain by an ~13-km-thick section of Cretaceous and Cenozoic sedimentary and volcanic deposits (Fig. 3; Dibblee, 1982a). In the Mesozoic and early Cenozoic, the Transverse Ranges block, or blocks, occupied the forearc region of a subduction zone collecting continental shelf sediments (Atwater, 1998). During the Oligocene, the Pacific plate made contact with North America (Atwater, 1998), and the tectonic regime in the Western Transverse Ranges changed as the San Andreas transform plate boundary (Fig. 1A) evolved over time (Crowell, 1979). In the middle Miocene, the configuration had a transtensional geometry that was responsible for localized extension, rotation, and left-lateral shearing (Atwater, 1998). Later, beginning in the Pliocene, the region began to undergo shortening (Atwater, 1998; Dibblee, 1982b; Rockwell, 1983); this shortening regime continues to the present (Rockwell, 1988; Rockwell et al., 1988; Marshall et al., 2013).

The sedimentary series is almost entirely marine, except for the Oligocene Sespe and late Quaternary Saugus Formations, implying

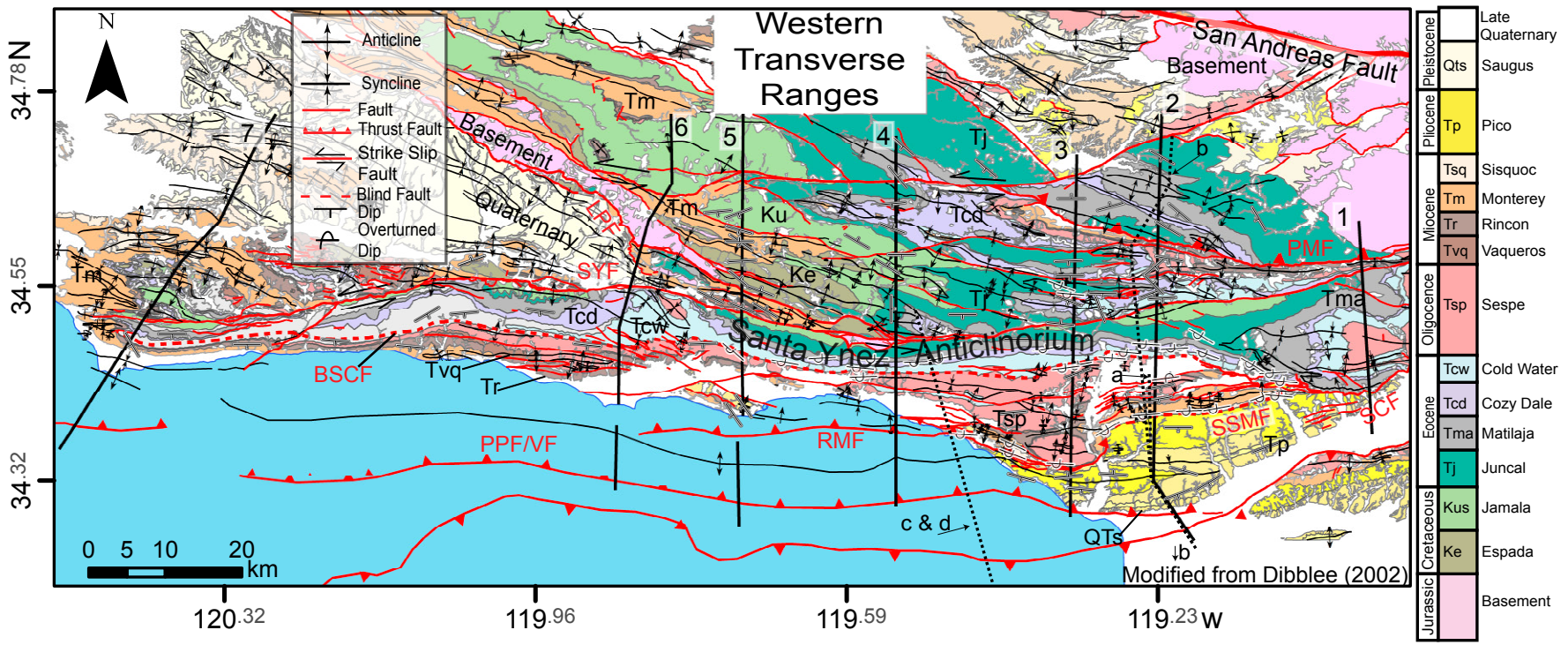

Figure 2. Geological map of the Western Transverse Ranges compiled from Dibblee (2002). The Santa Ynez anticlinorium and general east-west trend of the structures are apparent. Stratigraphic column is given in Figure 3. The stratigraphic column in this figure does not represent thickness, and it is missing some units that are outside the area of the cross sections; coloring of the geological units in the map is consistent with the column. Dip data are presented only as type and direction. Locations of the different cross sections are marked with black lines. Locations of previous model as presented in Figure 5 are marked with dotted lines and indicated by letters. The model presented by line b exceeds the limits of the figure to the south as marked by an arrow in the bottom right corner. SCF—San Cayetano fault; BSCF—blind San Cayetano fault; SYF—Santa Ynez fault; SSMF—South Sulphur Mountain fault; VF—Ventura fault; PMF—Pine Mountain fault; PPF—Pitas Point fault; RMF—Red Mountain fault.

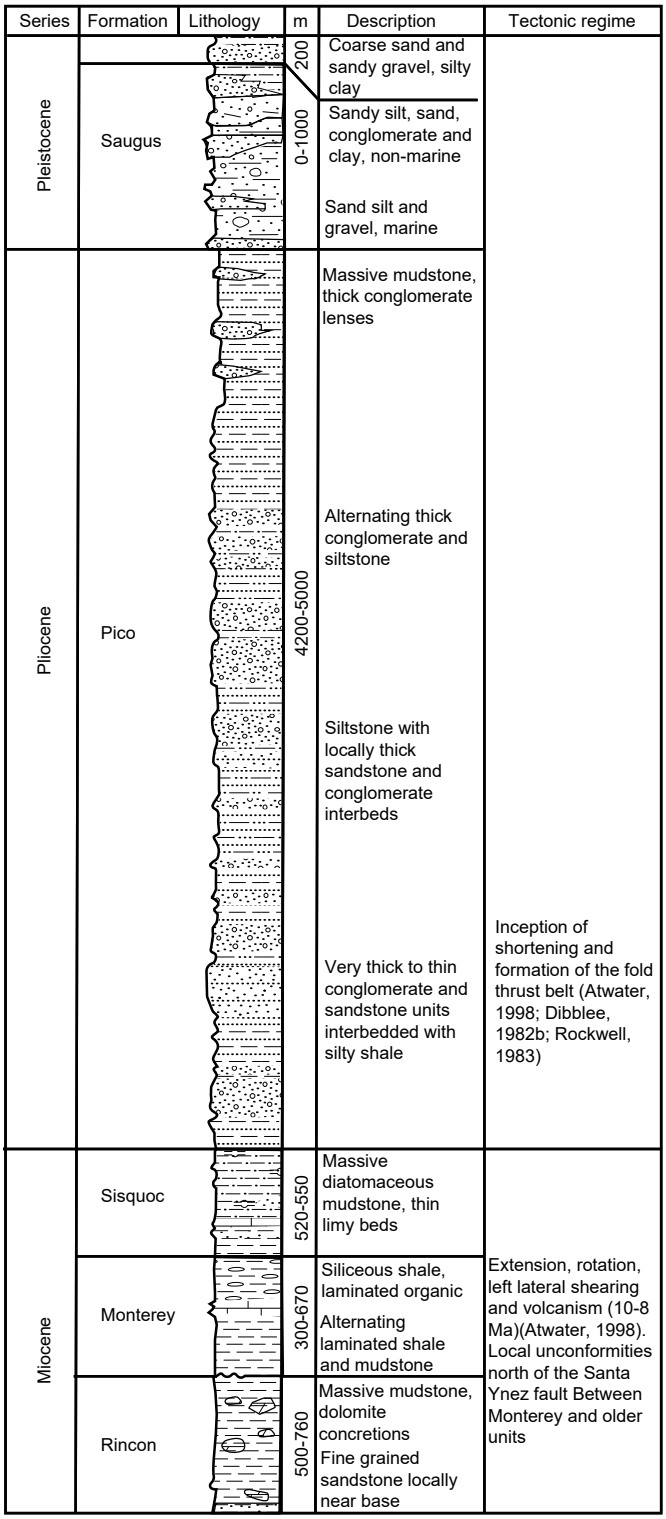

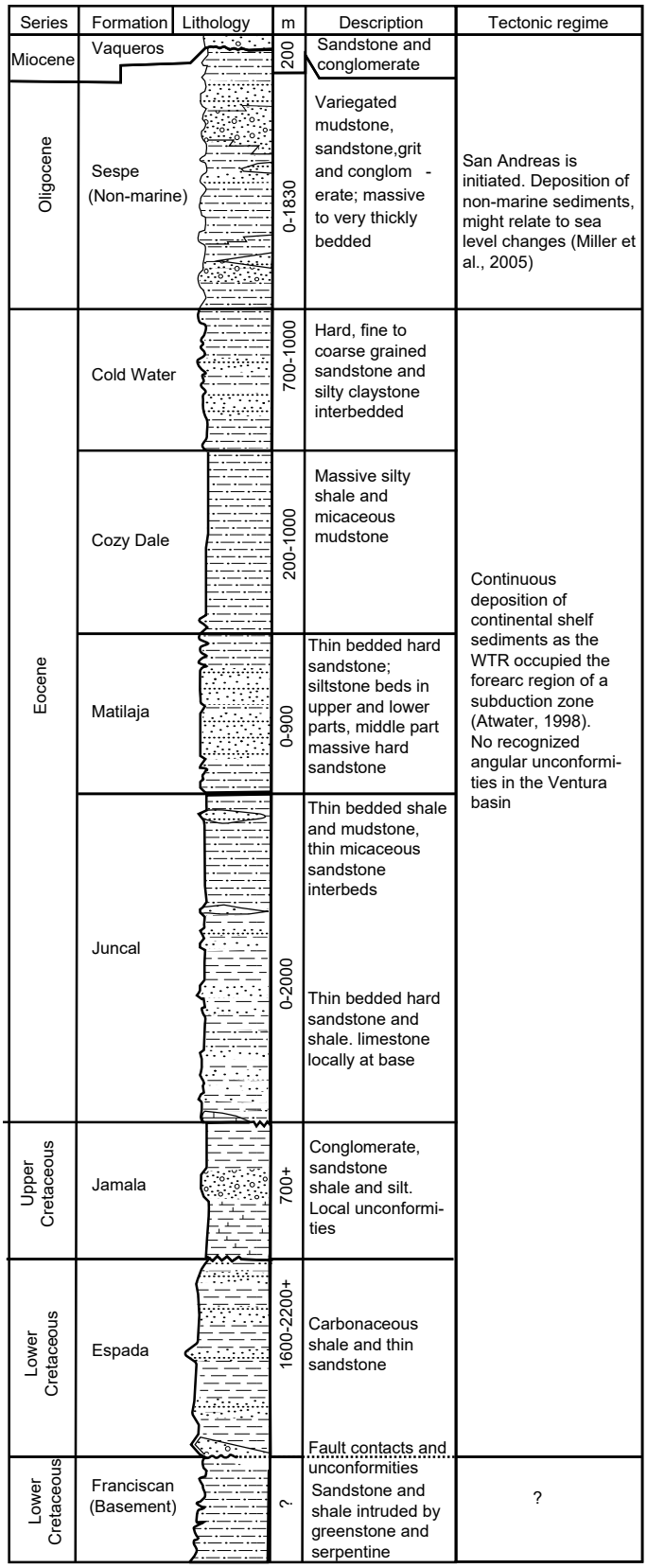

Figure 3. Stratigraphic column of the Western Transverse Ranges (WTR) modified from Dibblee (1982b). Thickness is presented in meters in the numerical column. This is a generalized stratigraphy, and some units have fault contacts as can be seen in Figure 2. For stratigraphic columns in different localities, we refer to Dibblee (1982b). We added a column that describes the tectonic regime.

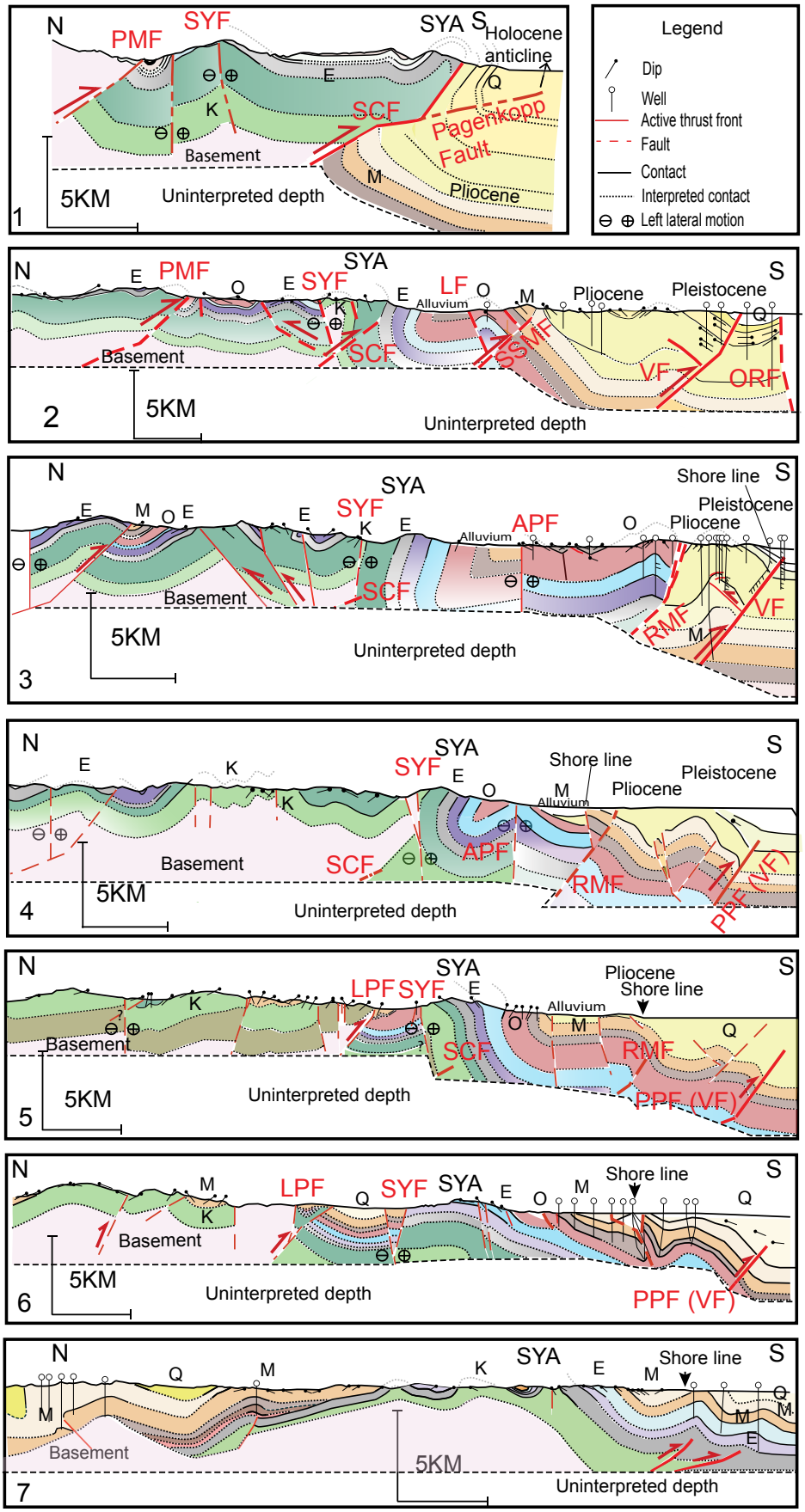

that the region has mostly experienced continuous subsidence. Bird and Rosenstock (1984) presented a case to explain the regional subsidence with a model of mantle downwelling and incipient subduction, which might explain the mechanism required to accommodate such a thick stratigraphic sequence. While the deposition of the terrestrial Oligocene Sespe sediments might imply uplift, global sea level changed during that period due to the formation of the large ice sheets in Antarctica (Miller et al., 2005).

Deposition in the Santa Barbara/Ventura Basin, south of the range (Figs. 2, 3, and 4), has been nearly continuous since the Eocene, and it accelerated in the Pliocene (Dibblee, 1982b; Yeats and Rockwell, 1991). Northward from the Santa Ynez fault system, the Eocene sequence thins rapidly, as do the Oligocene Sespe Formation and the Rincon and Vaqueros Formations (Dibblee, 1982b). An angular unconformity is locally present between the middle Miocene (Mohnian) Monterey Formation and older strata (Figs. 2, 3, and 4), which suggests a pre–late Miocene period of erosion that may have resulted from local uplift during Miocene extension. There are two models that describe the Miocene period of rotation and local extension, as indicated by paleomagnetic measurements (e.g., Hornafius, 1985; Hornafius et al., 1986, 1982; Nicholson et al., 1994; Schwartz 2018). One model suggests that the Western Transverse Ranges rotated clockwise by 110° as a large coherent block (Hornafius et al., 1982; Nicholson et al., 1994). Dibblee (1982b), referring to this earlier work (Hornafius et al., 1982), stated that so much rotation and the space problem with large adjacent blocks would be difficult if not impossible to account for from the geology. Alternatively, Schwartz (2018) suggested that the Miocene rotation more likely occurred as rotation of microplates. In either case, the paleomagnetic measurements show that most

Figure 4. Geological cross sections (locations in Fig. 2). The sections present mainly observations and some interpretation based on stratigraphic thickness from maps and Dibblee (1982a). The blind San Cayetano fault, as we interpret it, is not included in all the sections, as there are no direct observations of the fault west of Ojai Valley, and we did not interpret the full depth of the seismogenic zone. SYA—Santa Ynez anticlinorium. Geological units: K—Cretaceous; E—Eocene; O—Oligocene; M—Miocene; Q—Quaternary. Faults (red letter): SCF—San Cayetano fault; SYF—Santa Ynez fault; SSMF—South Sulphur Mountain fault; VF—Ventura fault; PPF—Pitas Point fault; LF—Lion fault; ORF—Oak Ridge fault; PMF—Pine Mountain fault; LPF—Little Pine fault; RMF—Red Mountain fault; APF—Arroyo Parida fault.

of the rotation accrued between 12 and 8 Ma (Hornafius et al., 1986; Schwartz, 2018), and therefore the rotation observed in the Western Transverse Ranges predated the current shortening regime, which began during the Pliocene.

Figure 2 presents a compilation of a large number of geologic maps of the Western Transverse Ranges (Dibblee, 2002). A first-order observation is that topography is being built to the north, and the structural relief from north to south is ~11 km with the north side up, as Cretaceous rocks are exposed along the Santa Ynez anticlinorium and Quaternary rocks are exposed to the south in the Ventura anticline and in the Ventura Basin (Figs. 2, 3, and 4).

The most obvious feature along the Santa Ynez mountain range is the ~160-km-long, E-W–trending Santa Ynez anticlinorium. This anticlinorium has a mostly overturned south limb, with a 5-km-thick section of overturned Eocene marine and Oligocene strata. East of Ojai Valley (Fig. 1B), the south limb is cut by the south-verging San Cayetano fault, which is interpreted as the emergent portion of the associated thrust underneath this fold (Namson and Davis, 1988). Where the San Cayetano fault is emergent, the fault displaces early Eocene rocks in the hanging wall against Quaternary rocks in the footwall with as much as 9 km of stratigraphic separation at the surface (Rockwell, 1988), although additional shortening by folding may require a larger basement offset.

The nomenclature in the Western Transverse Ranges is a source for confusion, so it is important to clarify that the Santa Ynez fault, in many locations, is too far north from the anticlinorium to be interpreted as the fault that produced this large fold (Fig. 2). Furthermore, the Santa Ynez fault currently exhibits mainly left-lateral strike-slip motion (Darrow and Sylvester, 1983), and it has a very steep dip that varies from dipping to the north to dipping to the south along its strike. Although its late Quaternary slip history is strike-slip motion, the Santa Ynez fault has sustained as much as 1–3 km of dip slip, which presumably occurred prior to its current role partitioning the majority of the strike slip accommodated within the Western Transverse Ranges.

There are a variety of structural interpretations for this region (Fig. 5). Yeats et al. (1988) presented balanced cross sections with a dominant north-verging structure, the Sisar décollement, at 8 km depth, south of the Red Mountain and San Cayetano faults. In their model (Fig. 5A), both the Ventura Avenue anticline and the Sulphur Mountain anticline, the latter of which is located between the Lion and South Sulphur Mountain faults (Fig. 1A), were formed by a south-dipping thrust system that roots to a décollement ~8 km under the surface.

Namson and Davis (1988) presented their model (Fig. 5B) based on fault-propagation fold and fault-bend fold methods (Suppe,1983). They proposed the presence of a detachment at 12–15 km depth and associated the San Cayetano thrust with the Santa Ynez anticlinorium. From seismological observations, a north-dipping low-angle fault was interpreted that might also relate to Namson and Davis' (1988) décollement at depths of ~12 km (Corbett and Johnson, 1982; Hauksson et al., 2016; Huang et al., 1996). South of the anticlinorium, the main thrust in the Namson and Davis (1988) model dips south, in what seems to be a structure that is comparable to the Sisar décollement presented by Yeats et al. (1988). Namson and Davis (1988) interpreted the South Sulphur Mountain anticline to result from the south-dipping Lion fault, and the Ventura Avenue anticline has a number of small layer-parallel faults, dipping alternately south and north, associated with it in their model.

Hubbard et al. (2014) applied fault-related folding theories (Shaw et al., 2005; Suppe, 1983; Suppe and Medwedeff, 1990) and used well and seismic reflection data in the Ventura Basin to construct a model of the Ventura Avenue anticline. They incorporated the Ventura fault as the structure producing the Ventura Avenue anticline, and they connected this fault with the Red Mountain, Lion, and San Cayetano faults, with a flat thrust within the Rincon shale at ~7 km depth. The linkage between the detachment and San Cayetano fault yields a ramp-flat-ramp geometry for the Pitas Point/Ventura fault. In this model, the structure forming Sulphur Mountain is also interpreted as a south-dipping fault. This model is represented as one version in the SCEC CFM5.2 (Fig. 5C; Plesch et al., 2007; Nicholson et al., 2017).

Sorlien and Nicholson (2015) presented several interpreted seismic cross sections in the offshore Ventura–Santa Barbara Basin but did not extend or interpret faults below the depth of imagery, i.e., ~6–7 km. Their sections demonstrate that the offshore Pitas Point fault system is aligned with the onshore Ventura fault and anticline. One of the versions of the SCEC CFM presents high-angle reverse oblique faults as the dominant structures producing the Western Transverse Ranges (Fig. 5D; Nicholson et al., 2017). Faults are connected as a regional flower structure in this version, and there is no blind San Cayetano fault west of Ojai Valley. This version appears to attribute the formation of the Santa Ynez anticlinorium to a south-dipping Santa Ynez fault, but this cannot be correct because the anticlinorium is overturned (verges) to the south, and the fault is far to the north.

TIMING AND STYLE OF DEFORMATION

The formation of the Santa Ynez anticlinorium probably initiated during the late Pliocene or early Quaternary (Dibblee, 1982a), and folding ceased before 200 ka (Rockwell, 1988). The age of initiation of the San Cayetano fault is not directly constrained. Rockwell (1983) documented that uplift to the north initiated by ca. 3.2 Ma, based on analysis of microfauna in the Lower Pliocene Pico Formation, which also contained clasts of the Miocene Monterey Formation that were derived from the north. These may have been shed from folding and uplift north of the Santa Ynez range, or from the anticlinorium itself. The south-verging, overturned Red Mountain anticline and north-dipping Red Mountain fault began motion by at least 1 Ma (Yerkes and Lee, 1987). The current dip on the Red Mountain fault is anomalous in that it dips steeply (70°) to the north, which is unfavorable for accommodation of shortening.

Folding of the onshore Ventura Avenue anticline is estimated to have begun around ca. 300–200 ka (Rockwell et al., 1984) and continues to the present (Hubbard et al., 2014; McAuliffe et al., 2015; Rockwell et al., 2016). In the offshore to the west, the same fold trend initiated motion earlier in the Quaternary and appears to be progressively older toward the west (Sorlien and Nicholson, 2015). This makes sense if the primary cause of folding in the Western Transverse Ranges is associated with the continued development of the Big Bend in the San Andreas fault (Crowell, 1979), as the westernmost Transverse Ranges toward Point Conception are now translated west of the Big Bend such that the shortening should have been earlier, and the current rate should be much lower. We discuss this further later in this paper.

The late Quaternary vertical motions are an important consideration in the development of a defendable structural model. North of the Arroyo Parida fault, terraces of the Ventura River (Fig. 1B, locality c) indicate regional uplift (without folding) at ~1 mm/yr across the southern flank of the Santa Ynez anticlinorium for at least the past 200 k.y. (Rockwell et al., 1984). Similarly, the Santa Ynez Valley north of the anticlinorium is rising at a similar rate of ~1 mm/yr (Fig. 1B, locality d; Farris, 2017). These observations argue for a regional uplift rate north of the Arroyo Parida fault of ~1 mm/yr, which must be accounted for in any viable structural model.

Farther west in the Santa Barbara region (Fig. 1B), current contractional deformation is also localized south of the Arroyo Parida–Mission Ridge fault, although the main topographic relief is to the north in the Santa Ynez Mountains

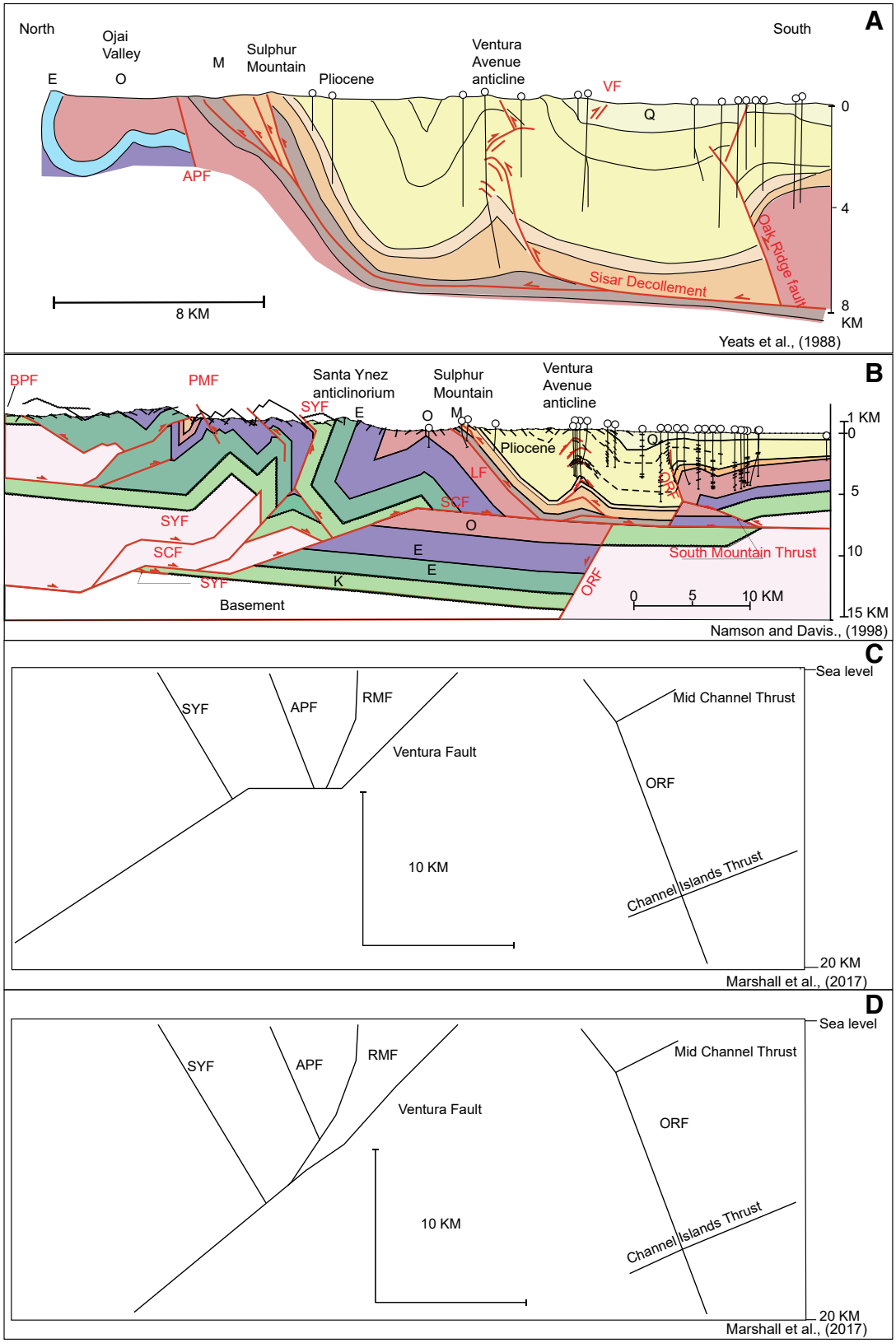

Figure 5. Previous structural and fault models for the region (locations in Fig. 2). (A) Cross section B-B′ of Yeats et al. (1988). (B) Cross section from (Davis and Namson, 1998), where Eocene is presented as one unit in purple. (C–D) Two versions of the Community Fault Model of the Southern California Earthquake Center (Nicholson et al., 2017; Plesch et al., 2007) for this region: the Hubbard model (C) and the flower structure model (D) as presented in Marshall et al. (2017). Cross sections and models were edited to match the color coding and abbreviations used in this paper. Geological units: K—Cretaceous; E—Eocene; O—Oligocene; M—Miocene; Q—Quaternary. Faults (red letter): SCF—San Cayetano fault; SYF—Santa Ynez fault; VF—Ventura fault; PPF—Pitas Point fault; LF—Lion fault; ORF—Oak Ridge fault; PMF—Pine Mountain fault; BPF—Big Pine fault; RMF—Red Mountain fault; APF—Arroyo Parida fault.

(Gurrola et al., 2014). Southward, active deformation extends offshore into Santa Barbara Basin, with active folding of the Pitas Point/Ventura Avenue, Red Mountain, Oak Ridge, and Mid-Channel anticlinal trends (Perea et al., 2017; Shaw and Suppe, 1994; Sorlien and Nicholson, 2015). The ca. 57 ka marine terraces demonstrate an uplift rate of ~1 mm/yr at Isla Vista (Fig. 1B, locality e; Gurrola et al., 2014) and at least 0.3 mm/yr farther west (Fig. 1B, locality f) between Gaviota and Point Conception (Rockwell et al., 1992). The apparent decrease in rate to the west is consistent with observed lower rates of shortening based on global positioning system (GPS) data (Marshall et al., 2013).

The most rapid rates of uplift in the entire region are associated with the Ventura–San Miguelito anticline at Punta Gorda (Fig. 1B, locality a), where the long-term rate is estimated at 6–7 mm/yr (Rockwell et al., 2016). This is also where four Holocene marine terraces have been identified, with each terrace interpreted to correspond to an abandoned abrasion surface due to uplift produced by an earthquake (Rockwell et al., 2016). The highest Holocene terrace is preserved at ~38 m above modern sea level near the fold crest and is interpreted to represent the cumulative uplift from four large earthquakes (Rockwell et al., 2016). In addition, analysis of GPS data showed that this region has the highest rate of shortening (fig. 5 *in* Marshall et al., 2013). Finally, results from a geodetic study showed an uplift signal north of the Santa Ynez range, which is consistent with interseismic strain accumulation on active thrusts in the Western Transverse Ranges (Hammond et al., 2018).

CROSS SECTIONS

We constructed seven geological cross sections over a 140 km length of the Western Transverse Ranges, from near Fillmore westward to near Point Conception (Figs. 2 and 4), using surface geology and dip data (Dibblee, 2002), subsurface well control (see Appendix), and seismic and previous geologic sections (Davis and Namson, 1998; Hubbard et al., 2014; Jackson, 1981; Namson and Davis, 1988; Sarna-Wojcicki and Yerkes, 1982; Schlueter, 1976; Sorlien and Nicholson, 2015; Yeats, 1983). Each cross section (Fig. 4) presents near-surface observations, and interpretations where surface data were projected downward to a small extent. Interpretations of thickness are based on calculations of true thickness from the geological maps (Dibblee, 2002) and from the stratigraphic columns presented in Dibblee (1982a). The overturned south limb of the anticlinorium is apparent in sections 1–5. To the west, in cross-section 6 and 7, the south limb is not overturned, but the anticlinorium still appears to be the largest structure.

The first-order observations of uplift in the north and subsidence in the south point to a southward-directed motion for the main faults at depth. These southward-verging faults are interpreted to accommodate the observed shortening and uplift. The models that consider the south-dipping faults as the dominant structures, such as the inferred Sisar detachment, which has been interpreted primarily as a tool to balance cross sections (Yeats et al., 1988), are thus inconsistent with the well-documented vertical motions of the region. Observationally, the Ventura–Santa Barbara Basin is subsiding at a high rate of 2–3 mm/yr, whereas onshore north of the basin, there are observations that argue for relatively high rates of uplift.

One aspect of our geological interpretation that is significantly different from previous interpretations (Fig. 5) relates to the fault that produces the South Sulphur Mountain anticline; the subsurface is poorly constrained by well control because most of the oil production has been from shallow strata. The regional orientation and alignment of the structures (Fig. 2), along with the overturned south flank (verges south) and stratigraphic relief, suggest that this anticline was produced by a north-dipping fault. In cross section 2 (Fig. 4), we interpret it as a south-verging structure, with the South Sulphur Mountain fault as the main thrust and the Lion fault as a back thrust, rather than the previously suggested interpretation of a dominant south-dipping fault (Hubbard et al., 2014; Namson and Davis, 1988; Yeats et al., 1988), which did not include the observed overturned south flank (Fig. 2; Dibblee, 2002).

Finally, our model seeks to explain the southward younging or serial development of the first-order structures, from early development of the Santa Ynez anticlinorium to the late Quaternary evolution of the onshore Ventura Avenue anticline, as described in the next section.

EVOLUTION OF THE FOLD-AND-THRUST SYSTEM SINCE THE PLIOCENE

When considering all of the observations referred to above on the timing and location of folding, it is apparent that the Western Transverse Ranges are a southward-propagating fold-and-thrust belt, as first suggested by Rockwell (1983), and that it is evolving in a fashion similar to other forward-propagating fold-and-thrust belts (Boyer and Elliott, 1982; Butler, 1987; DeCelles et al., 2001; Jordan et al., 1993; Morley, 1988; Wiltschko and Dorr, 1983), as also demonstrated in laboratory experiments (e.g., Storti et al., 1997; Smit et al., 2003). Onshore near Ventura, current deformation is localized between the Arroyo Parida fault (Rockwell et al., 1984) and the Ventura fault (Hubbard et al., 2014; McAuliffe et al., 2015), with the majority of shortening taken up by the Ventura Avenue anticline and associated Ventura fault. Offshore, east of Santa Barbara, the pattern is a little more complex based on new seismic reflection (CHIRP) data (Perea et al., 2017). The interpretation of these data suggests that the deformation has jumped from east to west and from south to north, from the Pitas Point/Ventura Avenue anticline and Pitas Point fault to the Red Mountain anticline and then to the Mesa–Rincon Creek fold system (located in Fig. 1B between locality e and Santa Barbara). Close to Ventura, the most active structures are the Pitas Point/Ventura Avenue anticline and Pitas Point fault, whereas the Mesa–Rincon Creek fold system is the most active structure close to Santa Barbara (Perea et al., 2017).

We conclude that a blind extension of the San Cayetano fault west of Ojai Valley produced the mostly overturned Santa Ynez anticlinorium as the first location of the thrust front, as first suggested by Namson and Davis (1988). North of the Santa Ynez range, the Pine Mountain fault might predate the San Cayetano fault, but the lack of age data or associated stratigraphic observations does not allow us to resolve this question at this time, and total shortening from this structure is minor compared to that of the anticlinorium to the south. The observation that folding had ceased prior to 200 ka implies that the blind San Cayetano fault west of Ojai Valley (Fig. 1B) is no longer active. By at least 1 Ma (Yerkes and Lee, 1987), the thrust front propagated south, first to the Red Mountain and South Sulphur Mountain faults, and then, in the late Quaternary, to the currently active but mostly blind Pitas Point/Ventura fault, with the Pitas Point/Ventura Avenue and related anticlines developing in the hanging wall. The Red Mountain fault continues to play a role in the offshore Santa Barbara Basin, but onshore, we interpret the late Quaternary deformation and steep dip of the fault to be the result of passive flexural slip due to folding in the back limb of the Ventura Avenue anticline, similar to the schematic development of the imbricate thrust system presented by Poblet and Lisle (2011). This sequence of events for the onshore Ventura Basin is consistent with other well-documented fold-and-thrust belts worldwide, where propagation of the thrust front develops "in sequence" with the direction of vergence of the primary structures. Figure 6 illustrates our proposed model for the evolution of the first-order

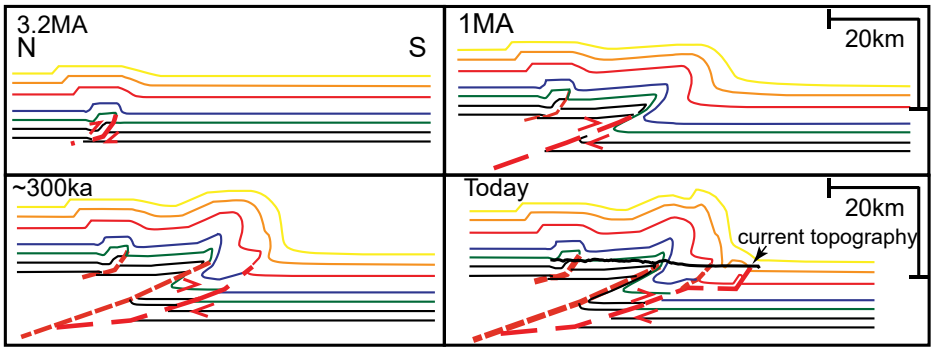

Figure 6. Trishear forward model showing the evolution of the fold-and-thrust belt system in the Western Transverse Ranges since late Pliocene time for cross section 2 (Fig. 4) as the thrust front has migrated south in the direction of vergence. Dashed red lines mark faults; thin colored lines represent rough approximation for contacts of footwall stratigraphy; thick black line in the last plot (present) represents the current topography. Colored lines demonstrate the resulting modeled deformation across the section and can be compared to the observed folds and dips. We did not model out-of-sequence thrusting; therefore, faults in the model are no longer active once a new thrust is superposed. Preexisting deformation was modeled in first panel (3.2 Ma), while secondary or out-of-plane deformation was mostly neglected. The result after cutting the lines with topography is presented in Figure 9; similar steps were performed for the other cross sections, and the final result was compared to surface and near-surface observations (Fig. 10).

Pliocene structure of the Western Transverse Ranges fold-and-thrust belt.

MODEL ASSUMPTIONS

We made a number of assumptions to model the geometry and evolution of faults at depth. The stratigraphy in the model is simplified, and the thicknesses of the units are fixed, although in the real world, there are local changes due to the Miocene period of rotation and extension. Considering that our goal was to model the overall first-order, Pliocene and younger contractional deformation of the Western Transverse Ranges, we suggest that the resulting mismatches from not incorporating these stratigraphic details are minor.

The second assumption is that out-of-plane motion can be neglected. Some faults in the Western Transverse Ranges have accommodated some strike-slip motion during the late Quaternary, and the larger earthquakes in the Central Transverse Ranges, to the east of the study area, have exhibited up to 30% left-lateral strike-slip motion (cf. the 1971 San Fernando earthquake). However, the orientation of shortening relative to the stress field generated by the Big Bend of the San Andreas fault argues that the maximum compressive stress is N-S (Rodgers, 1975), and this is borne out by modern geodetic observations that demonstrate primarily NNW-SSE shortening across the Western Transverse Ranges (Marshall et al., 2013), which, if anything, should produce a very minor right-lateral component of motion on E-W–striking faults. Thus, the amount of strike-slip relative to the rate of shortening is expected to be small, but we address it further here to avoid the common criticism of two-dimensional (2-D) modeling where there is a potential component of strike-slip motion.

The three high-angle strike-slip faults that may impact our forward modeling are the Big Pine, Santa Ynez, and Arroyo Parida faults (Fig. 1B). There are few data on the recent activity of the Big Pine fault, although it is sufficiently north of the main structures that any strike-slip motion will have negligible effect. The Santa Ynez fault has been studied to some degree with paleoseismic trenches; Darrow and Sylvester (1983, 1984) excavated a "box trench" (two perpendicular and two parallel trenches across a fault) to estimate 5–10 m of left-lateral displacement of basal terrace gravels, which are overlain by several meters of sediment and capped by a middle Holocene soil, which in turn provides a minimum age of displacement of ca. 5 ka. The next higher terrace (Qt2) has an estimated soil age of ca. 16 ka, placing a maximum age on the basal gravels. Thus, the maximum late Quaternary slip rate range for the Santa Ynez fault is estimated to be 0.3–2 mm/yr.

The Arroyo Parida fault displays no evidence of lateral slip in late Pleistocene terraces of the Ventura River (Fig. 1B, locality g; Rockwell et al., 1984), although a minor component could have been missed at the scale of mapping (1:20,000). Near Carpinteria (Fig. 1B, locality h), fluvial channels incised into bedrock in the Santa Ynez range display left deflections where the channels cross the Arroyo Parida fault. However, the bedrock channels must predate the last interglacial marine terraces, which cut across rock downstream from the fault crossings and are likely considerably older. Based on these observations, it does not appear that the Arroyo Parida fault has sustained much, if any, late Quaternary lateral slip at the Ventura River, and it likely has a low rate of well less than 1 mm/yr near Carpinteria and Santa Barbara. We consider both the Santa Ynez and Arroyo Parida faults as the structures that accommodate the partitioned strike-slip motion in the Western Transverse Ranges.

Seismological data also argue for a component of lateral slip, as most of the larger Transverse Ranges earthquakes exhibited oblique slip, based on observations from surface ruptures (Keller and DeVecchio, 2013) or focal mechanism solutions (Corbett and Johnson, 1982), although many of these observations are far to the east. In summary, there is a lateral component of shear in the Western Transverse Ranges, but considering a rate that is most likely less than 2 mm/yr, versus a contraction rate of that is close to 10 mm/yr, the lateral slip is considerably subordinate to the rate of shortening. Considering that the shortening of the Western Transverse Ranges initiated at ca. 3–2 Ma, there has been only a few kilometers of lateral shear during the period of contraction. In contrast, the Paleogene sedimentary rocks show lateral continuities on the scale of tens of kilometers with gradual thinning to the north in the direction of contraction. Therefore, the lateral component of strains should have only a minor effect on forward modeling that assumes pure contraction, especially for the pre-Miocene strata, which record the major shortening associated with the Santa Ynez anticlinorium.

Similarly, the thicknesses of most of the Neogene rocks to the top of Miocene are relatively constant, although there are exceptions due to extensional faulting during the Miocene, which are accounted for in the model. This is evident from the relatively constant thickness of marine units that form the Santa Ynez range from Point Conception to at least the Ventura River, with local areas of complexity. Based on the above discussion, we assume that the effects of out-of-plane motion are negligible for our forward modeling, as presented below.

ESTIMATE OF DIP FOR THE FAULT AT DEPTH

There is a considerable debate as to whether the structures in the Western Transverse Ranges are controlled solely by high-angle reverse oblique faults (Nicholson et al., 2017) or whether there is a regional detachment or gently dipping thrust ramp that underlies the region (e.g., Namson and Davis, 1988; Shaw and Suppe, 1994).

As mentioned in the geological background section, Namson and Davis (1988) presented evidence for placing a décollement at a depth of 12–15 km depth, and seismological observations support this interpretation (Corbett and Johnson, 1982; Hauksson et al., 2016; Huang et al., 1996). Hubbard et al. (2014) proposed the existence of a flat at ~7 km, in contrast to previous models with a south-dipping detachment under the basin (Namson and Davis, 1988; Yeats et al., 1988). Hubbard et al.'s (2014) flat was interpreted to connect a high-angle deep ramp of the San Cayetano fault to the Pitas Point/Ventura fault system via the "southern San Cayetano fault." Recent work has established that the southern branch of the San Cayetano exists, and it is the likely surface linkage between the San Cayetano and Ventura faults (Hughes et al., 2018). The geometry presented by Hubbard et al. (2014), which includes an ~30°N-dipping thrust ramp that extends downward from the flat, was favored over the high-angle reverse faults model by mechanical modeling (Marshall et al., 2017). The north-dipping thrust ramp proposed by Hubbard et al. (2014) provides a reasonable mechanism to explain uplift in the Western Transverse Ranges. However, it has yet to be tested against the observed regional uplift of ~1 mm/yr north of the Arroyo Parida fault (Rockwell et al., 1984) and in Santa Ynez Valley (Farris, 2017), or the lack of late Quaternary folding of the Santa Ynez range. Therefore, we explored this further, and we suggest that this deeper ramp must be more gently dipping to the north to account for the regionally observed uplift.

We estimated the plausible dip range by accounting for the rates of vertical and horizontal motion using a simplistic kinematic model (Fig. 7A) that assumed that the observed uplift north of the zone of active folding is a result of slip on the underlying, deep low-angle thrust. Regional subsidence due to mantle downwelling (Bird and Rosenstock, 1984) is also accounted for in the model. The subsidence rate was evaluated assuming that the Upper Quaternary coarse clastic sediments in Ventura Basin were originally at or close to the surface and that their current depth is the result of subsidence. Their ages have been previously defined by the presence of tephras and fossil extinction horizons (Yeats, 1983), so a subsidence rate could be calculated. Using the top of the Repetto member of the Pico Formation onshore between the Ventura and Oak Ridge faults results in a subsidence rate of ~2.6 mm/yr for the onshore central trough of Ventura Basin. For the offshore, the depth to the top of the Repetto member resolves a rate of ~2.5 mm/yr. The 2.5 mm/yr rate was used in our model as an estimate of the regional subsidence rate, although this rate might be considered as a maximum rate, in case subsidence is faster in the basin due to sediment loading, which is likely the case. In such a case, the calculated dip angle that we used may also be a maximum dip angle.

We employed shortening rates of 6.5–10 mm/yr determined from previous geologic and geodetic studies (Marshall et al., 2013; Rockwell et al., 1988) and our estimate of the change in line length of a horizon at the top of the Pico Formation in the Ventura area, south of the Red Mountain fault (Fig. 4, cross-section 3). The required dip of the lower fault ramp based on our model is shown by the intersection of each line and the 1 mm/yr uplift rate (Fig. 7B). The range of plausible dips is 16°–30° when accounting for the uncertainties in the shortening and uplift rates. In our models, we used a dip of 20° for the deep ramp, which is similar to the dip inferred for the fault that produced the Fillmore earthquake swarm based on microseismicity (Hauksson et al., 2016), as well as the dip of the fault that produced the 1978 M 6 Santa Barbara earthquake (Corbett and Johnson, 1982).

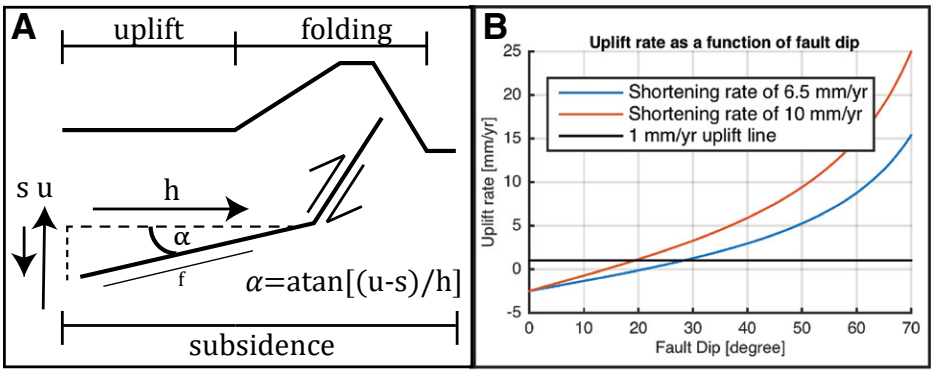

Figure 7. (A) Model used to calculate the fault dip for the lower ramp. Parameters: α—fault dip; h—horizontal shortening rate; u—uplift rate; s—subsidence rate. We assumed that competing rates of uplift and regional subsidence will equal the observed rate of uplift where there is no folding. (B) Plot of dip vs. observed uplift rate for different shortening rates and a subsidence rate of 2.5 mm/yr. The prediction for fault dip is at the intersection of the results (red and blue curves) with the 1 mm uplift line (black), which is the reported regional uplift. See text for further information.

FORWARD MODELING

In order to test the interpretation of a southward-propagating fault system and estimate the first-order geometry of the deep faults of the fold-and-thrust belt, we applied fault-bend folding (Suppe, 1983) and Trishear (Erslev, 1991) forward modeling. The results of the models were compared with and tested against the geologic cross sections presented in Figure 4. This comparison allowed us to assess whether a large deep thrust ramp may plausibly represent a continuous fault surface along strike that is capable of hosting large earthquakes.

We generated a series of kinematic forward models using the Trishear (Erslev, 1991) module in MOVE® by Midland Valley Exploration Ltd. (https://www.mve.com/) to match the surface and near-surface geology. We modeled a southward-propagating fault system by iterative steps. That is, we first produced slip on a fault to the north of the Santa Ynez anticlinorium to match some of the deformation in the hanging wall of the San Cayetano fault. We then "propagated" the deformation southward by initiating slip on a new fault to represent the San Cayetano fault, followed by the Red Mountain–South Sulphur Mountain fault, and finally the Pitas Point/Ventura fault system. We iterated this with various fault configurations until we matched the surface geology as interpreted in our geologic cross sections.

The order of faulting has an important impact on the patterns of resulting deformation, so representation of the regional evolution of structures in our models, as described above, provided an important constraint. Earlier stages of our models represent initial conditions that were then modified by subsequent faulting and folding. After each modeling step, we made an adjustment to the fault geometry and displacement parameters until we reached a satisfying result under the different constraints of age, geometry, and amount of shortening; hence, this was an iterative process. In Figure 6, we present the steps we applied for cross section 2 (Fig. 4); a similar procedure was performed for each of the other cross sections.

We used the same parameters for the different modeled sections except for fault spacing and fault displacement. The extent to which the thrust front propagated toward the south through time is apparent in Figure 2, as the distance between the San Cayetano, Red Mountain/South Sulphur Mountain, and Pitas Point/

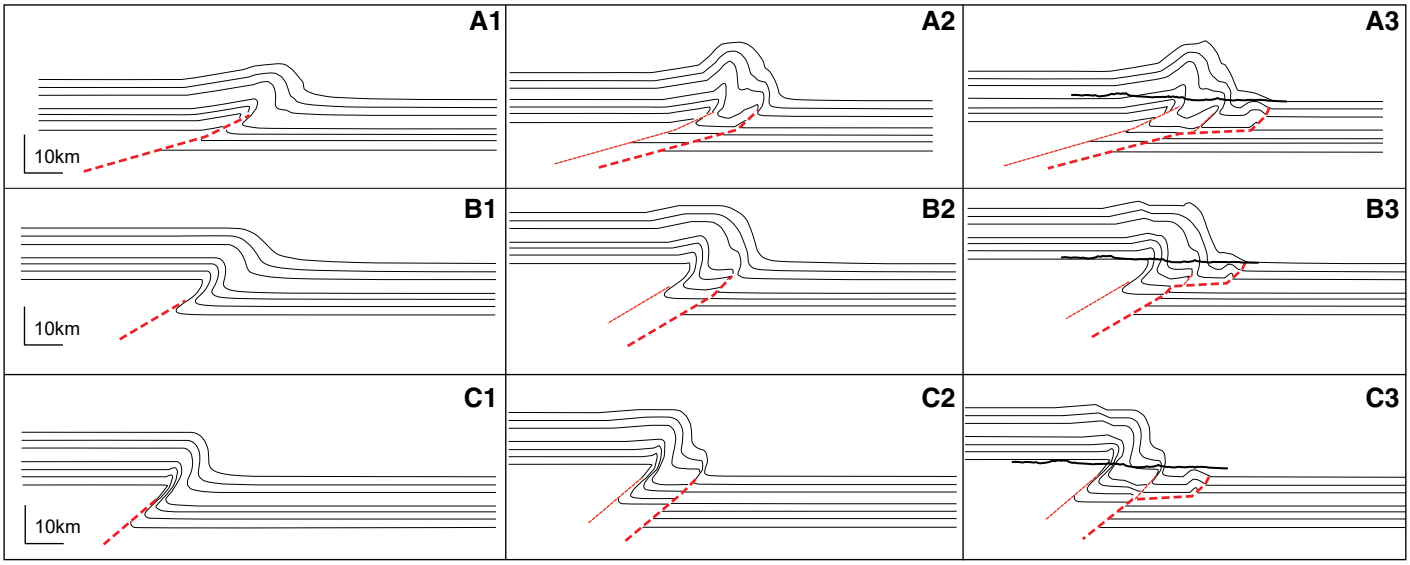

Figure 8. Models that present different dips for the lower ramp. Thick dashed red line is the fault that slipped most recently, whereas the thinner red line is an older inactive thrust, the thin black lines represent hypothetical contacts, and the thick black lines in A3, B3, and C3 represent the current topography. For these models, we used the same parameters as described in the text for the model presented in Figure 6. Model A1–A3 presents a deep ramp dipping 15° degrees north. Model B1–B3 presents a deep ramp dipping 30° degrees north. Model C1–C3 presents a deep ramp dipping 40° degrees north. The 40° dip is beyond our estimated range of likely dips as it does not well represent the known geology.

Ventura faults changes along strike. The amount of slip, or contraction, used in the models varied as overall shortening decreased to the west, so slip was reduced for cross sections 5, 6, and 7 to match the amount of deformation represented in the surface and near-subsurface geology.

The parameters we used for the final model are: For the San Cayetano fault, we used a propagation to slip ratio of 1, we used 20 Trishear zones, and we did not apply an offset for the Trishear angle. For the Red Mountain/South Sulphur Mountain fault, we used a propagation to slip ratio of 0.8 with 8 Trishear zones, and an offset of 0.6 for the Trishear angle. For the Pitas Point/Ventura fault, we used propagation to slip ratio of 0.3, 1 Trishear zone, and an offset of 0.9 for the Trishear angle. The propagation to slip ratio for each fault was selected to match the shape of the fold as best we could through trial and error; we did not thoroughly explore the sensitivity of this parameter. Figure 8 presents additional models using different dips than our preferred model for the lower ramp in order to demonstrate the sensitivity of relief and fold shape on the geometry of the lower ramp.

RESULTS

The model (Fig. 6) illustrates the concept of southward thrust propagation over time, attendant fault dip, and expected patterns of uplift and folding, with uplift of the hanging wall and the locus of folding migrating southward through time. The comparison of the model predictions with the geological cross sections shows a good first-order match and demonstrates that the models capture the first-order patterns of folding and structural relief (Figs. 9 and 10). Despite having a rather large spacing between cross sections, the similar fault geometry inferred at depth, along with the interpreted structural evolution through time, reproduces the surface dips of the anticlinorium and the younger anticlines to the south as the thrust front progressed south along the 140 km length of the range covered by the cross sections. Furthermore, the structural relief and stratigraphy in the forward models match

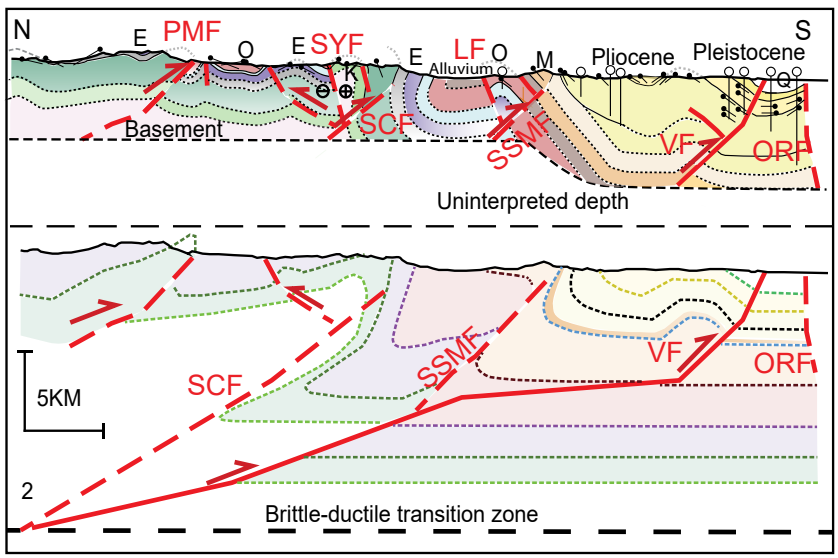

Figure 9. Comparison between geological cross section 2 (upper cross section) and the Trishear forward model (lower cross section) showing a good first-order match between the two. See Figure 2 for location of the cross section. Stratigraphy was simplified in the model. For abbreviations, see Figure 4. In the model, the thin colored lines represent rough simplified approximation for contacts of footwall stratigraphy.

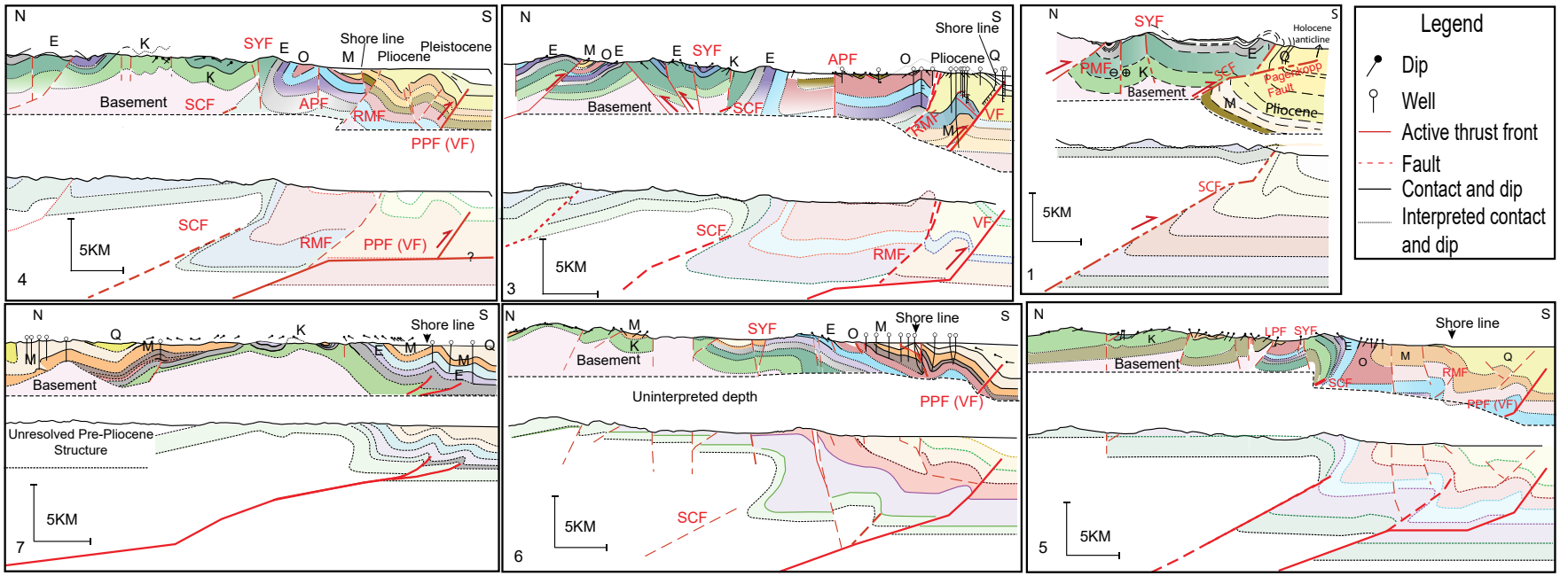

Figure 10. Comparison between the geological cross sections (upper cross section) and the Trishear forward model (lower cross section) for cross sections 1 and 3–7 showing a good first-order match between the two. See Figure 2 for locations of the cross sections and Figure 9 for deeper structure of sections 3–6. For abbreviations, see Figure 4. In the model, the thin colored lines represent rough simplified approximation for contacts of footwall stratigraphy.

well with the geologic cross sections constructed using classical techniques.

In our modeling, we included the sequence of events and ages of structures, as presented or determined in previous studies. There is some shortening represented by folding north of the San Ynez range, mostly associated with the Pine Mountain fault (Fig. 2), but the first major thrust front along the length of the Santa Ynez anticlinorium resulted from initiation of motion on the San Cayetano fault. This was followed by propagation of the thrust fault southward to the Red Mountain–South Sulphur Mountain fold and later to the Pitas Point/Ventura fault, all of which formed the imbricated thrust and ramp architecture as depicted in Figure 9. In cross-sections 2 through 5 (Figs. 9 and 10), there is a flat between the emergent Red Mountain and Ventura frontal faults, as modeled and interpreted by others (Hubbard et al., 2014; Namson and Davis, 1988; Shaw and Suppe, 1994; Yeats et al., 1988,) and we reproduced the low-angle flat in our modeling. In fact, we tried to eliminate this midcrustal flat and found that it was required in order to retain connectivity and simultaneously reproduce the surface geometry. The presence of the flat is also favored by mechanical models that analyzed geodetic data for the presence or absence of a midcrustal flat (Marshall et al., 2017).

Cross-section 1 (Fig. 10) required a simple geometry, compared to the other cross sections, without a ramp-flat-ramp structure. This was expected because there is no major fold south of the San Cayetano fault near Fillmore (Fig. 1B); a simpler structural configuration required a simpler structural evolution and model. It might be expected that the marginal cross section would exhibit a different geometry close to the lateral boundaries of the system. That said, a young fold emerges out of the late Quaternary alluvium west of Fillmore and south of the San Cayetano fault (Rockwell, 1988; Hughes et al., 2018) that was too small to model at the scale of the model, but it does represent the very recent southward propagation of the San Cayetano fault, as demonstrated by Hughes et al. (2018).

Based on these models, we estimated that ~21 km of total shortening has accrued since contraction began in the Pliocene in the eastern part of the Ventura Basin (cross-sections 1–4). The required shortening decreases to ~13 km in cross-section 5, ~11 km in cross-section 6, and ~7 km at the westernmost cross-section 7 near Point Conception. The average shortening rate implied by this amount of shortening, considering the age uncertainty, is 6.5–9.1 mm/yr for cross sections 1–4, in close agreement with geodetic estimates, which suggest an average current shortening rate of 7 mm/yr (Marshall et al., 2013), and geologic estimates of 8–10 mm/yr (Rockwell et al., 1988). Another factor of note is that the geodetic estimates of shortening in the westernmost Western Transverse Ranges (area of cross-section 7) are much lower than near Ventura (Marshall et al., 2013), consistent with our estimate that only a third of the shortening is required to produce the observed structures for the area of cross-section 7.

This reduction in shortening westward is consistent with the observation that the anticlinorium is not overturned west of cross-section 5 (Figs. 2 and 4), which also argues for a lesser amount of total shortening. The alternative is to place the main fault deeper, but the observation that the depth of microseismicity in the Western Transverse Ranges seems to shallow from east to west indicates that the seismogenic depth also shallows from east to west (Nazareth and Hauksson, 2004). This contradicts deepening the location of the main lower ramp and thus supports our decision to match the observed folding patterns with a westward decrease in slip.

The westward decrease in the amount of shortening is likely the result, in part, of the position of the westernmost Transverse Ranges relative to the Big Bend of the San Andreas fault, which has evolved over time. Early in the history of contraction (late Pliocene?), the region around Point Conception would have been far to the east of its current position because of less total slip on the San Andreas fault. Therefore, the contraction in the west may be older, resulting from the previous location of this region directly south of the Big Bend in the San Andreas fault. Furthermore, the Big Bend of the San Andreas, which is inferred to be a major factor in contraction in the Western Transverse Ranges, has evolved over time as slip accrued on the Garlock fault (Fig. 1A) from extension in the Great Basin (Davis and Burchfiel, 1973).

Full agreement between model prediction and geologic observations is unrealistic for a number of reasons. First, changes in thickness are observed as units thin to the north, and it is difficult to model this aspect accurately in Trishear. In addition, secondary structures and additional deformation resulting from minor back thrusts and from out-of-plane strike-slip faulting are difficult to quantify, although the amount of strike-slip motion is minor compared to dip slip, and the initial geometry of the Paleogene section was relatively simple. Finally, the superposition of the present compressional deformation regime on the Miocene extensional regime is another factor that introduces additional complications. For example, the Miocene growth strata and sections that were eroded make it difficult to compare the observed geology to a simple layered model. The simplifications we made, mainly using a layer cake model, might affect the amount of total shortening we used in the model. In the case that the Lower Eocene or Cretaceous units already had some relief from north to south, a lower dip or slip on the modeled faults would have been required, and vice versa. Because we have no way to constrain the paleorelief of these units, we cannot quantify this uncertainty, although there are no clastic deposits eroded from the Eocene strata in the Miocene units, which argues against subaerial exposure of the Eocene strata to the north. Considering those issues, and accepting the limitations of our inherent assumptions, we suggest that our structural models reproduce the geometry and kinematics of the major thrust sheets, and they are consistent with all large-scale observations along the transects (Figs. 9 and 10).

THREE-DIMENSIONAL FAULT SURFACE

Considering that the depth of the brittle-ductile transition in the Western Transverse Ranges is as deep as 18–20 km, based on depth distribution of the seismic moment release (Nazareth and Hauksson, 2004), we can estimate the fault surface area for the underlying thrust. Figure 11 presents an interpolated fault surface (using the spline curve method) for that portion of the crust that lies in the seismogenic zone. In this three-dimensional (3-D) model, we connected the various fault lines with the assumption that the active deep fault connects to the frontal fold-and-thrust zone as one continuous thrust surface. Based on this model, we estimated that the surface area of the fault is ~6000 km^2. If the entire ~140 km length of the fault system fails in a single event, an earthquake in the Mw 7.8 range is possible, based on scaling relations (Leonard, 2010). As the slip rate, and therefore expected slip per event, decrease to the west, this is likely a maximum estimate of the plausible earthquake magnitude.

This magnitude of potential earthquake, or at least a magnitude in the Mw 7.5–7.8 range, is supported by the aforementioned recent studies of coastal uplift, borehole excavations, and structural analysis (Hubbard et al., 2014; McAuliffe et al., 2015; Rockwell et al., 2016). The Holocene coastal marine terraces near Punta Gorda between Ventura and Santa Barbara record Holocene uplift events that average 10 m (Rockwell et al., 2016). Similarly, the onshore Ventura fault has produced up to 6 m of vertical deformation per event (McAuliffe et al., 2015). These amounts of uplift in a single event are only known worldwide from large earthquakes.

The evidence for large displacements or uplift led Hubbard et al. (2014) to propose that

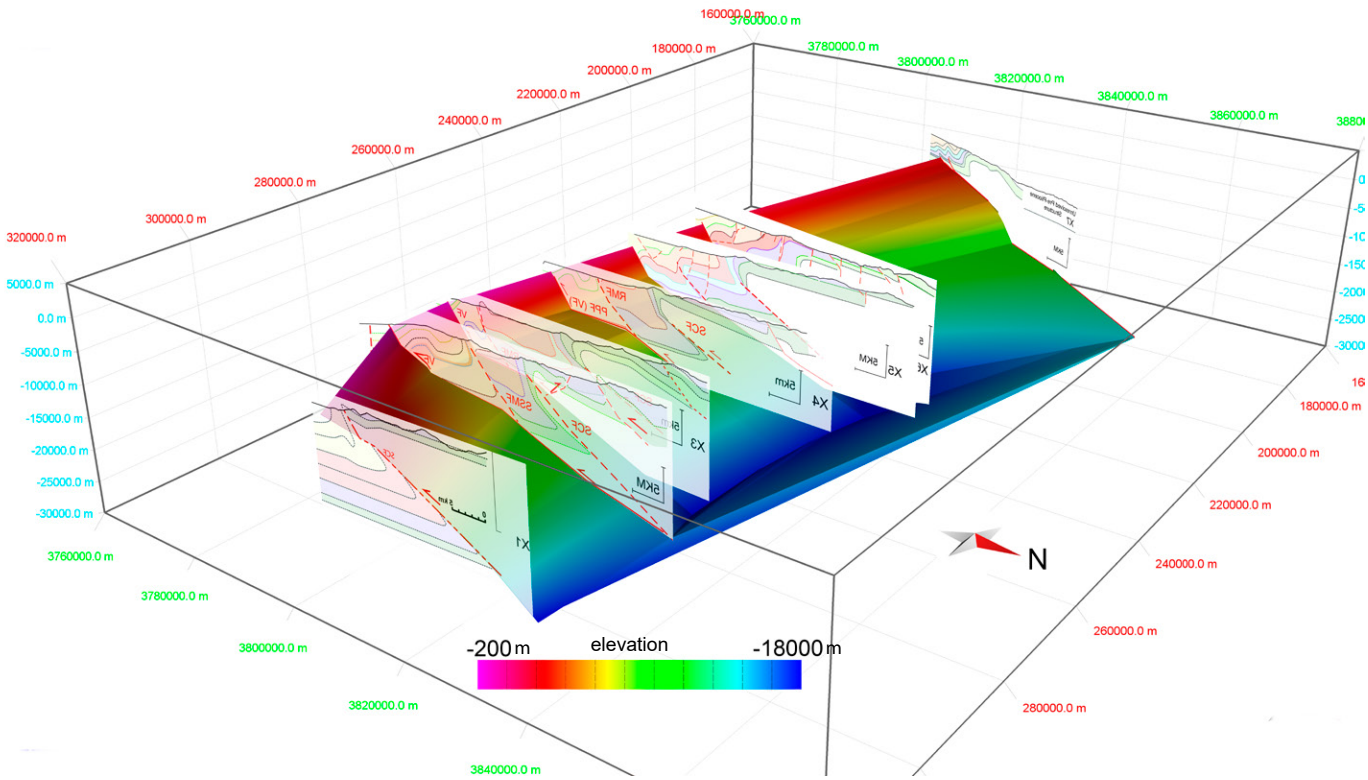

Figure 11. Interpolation of the predicted active fault surface. Surface was interpolated from the modeled fault lines using spline curve method down to the seismogenic depth (18 km; Nazareth and Hauksson, 2004). The surface area of the fault is estimated at ~6000 km², which can potentially host a high 7 magnitude earthquake according to scaling relations (Leonard, 2010).

some ruptures must involve multiple segments to accommodate the expected surface area of such uplifts. They argued that rupture of just the emergent portion of the San Cayetano and Ventura faults was too small to explain such large events, and thus proposed multisegment ruptures that extended east and/or west. Our interpretation for the surface area of the thrust is about twice that of Hubbard et al. (2014) due to the shallower dip of the lower ramp down to 18–20 km depth and extension of the fault system to the west. Thus, our fault representation is of sufficient size to host the class of earthquakes that independent paleoseismic data indicate have occurred within the system.

One other aspect is worth noting. The low dip that we infer for the underlying thrust ramp in our model predicts that a geodetic uplift signal should be observable to the north of the Santa Ynez range, contrary to that from the steeper dips inferred for other models (Sorlien and Nicholson, 2015; Nicholson et al., 2017). Our model is consistent with the geodetic uplift signal north of the Santa Ynez range (Hammond et al., 2018), which indicates that the deep thrust related to the shortening at the brittle-ductile transition zone is in the same area as we predict.

CONCLUSIONS

Based on our new kinematic forward modeling effort, we propose that the primary structures of the Western Transverse Ranges result from a southward-verging system of folds and thrust faults that have evolved through time. In our model, the lower ramp dips ~20° (with possible range of 16°–30°) to the north, to explain the regional uplift of 1 mm/yr, and the upper ramp dips ~45°–60° to the north, based on well data. Based on seven forward models (Figs. 9 and 10) that explain well the observed surface geology and interpreted cross sections, we infer that the deep structure is best represented by a large, continuous thrust sheet that connects the various geological structures observed at the surface. The presence of this large, interpreted fault can explain the large deformations that have been documented for the Pitas Point/Ventura fault system at the coast. The potential surface area of a rupture in the seismogenic zone may be as large as ~6000 km²; such a scenario could yield an earthquake as large as M 7.8 (Hubbard et al., 2014; McAuliffe et al., 2015; Rockwell et al., 2016). Further, we predict that the rate of shortening drops significantly in the offshore from east to west, which implies that displacement per event also likely falls off to the west.

Finally, our approach of accounting for observations that constrain the model but do not serve as inputs might be applied in other fold-and-thrust belts worldwide. Independent information on fault slip rates, uplift and shortening rates, relative timing of structures, geodetic data, and other independent information help to guide the development and restrict the degrees of freedom for structural models of the entire seismogenic crust, as in our models for the Western Transverse Ranges.

APPENDIX: WELL DATA

In Appendix Table A1, we include the API numbers and coordinates for the wells we incorporated into our cross sections. Some of the wells were interpreted by the studies cited in our work, while others had a well log available through the Department of Conservation, California, website (https://maps.conservation.ca.gov/doggr/wellfinder/#close).

ACKNOWLEDGMENTS

This research was supported by the Southern California Earthquake Center (SCEC), Contribution 8054. SCEC is funded by National Science Foundation Cooperative Agreement EAR-1033462 and U.S. Geological Survey Cooperative Agreement G12AC20038. H. Perea was supported by the European Union's Horizon 2020 research and innovation program under grant H2020-MSCA-IF-2014 657769. We thank Alex Hughes, Dylan Rood, Scott Marshall, and Nate Onderdonk for interesting and helpful discussions, and we thank Edward Keller and Vikash Tripathy for excellent reviews of an early version of this manuscript.

APPENDIX TABLE A1. WELL DATA

API	Longitude (°W)	Latitude (°N)
11105289	119.297089	34.31761
11120851	119.226167	34.31161
11103876	119.297111	34.309279
11105923	119.229634	34.295784
11105917	119.218798	34.292384
11104005	119.268814	34.28971
11105919	119.190851	34.290011
11104006	119.269424	34.28689
11105811	119.306094	34.285428
11106169	119.316914	34.283682
11120500	119.207144	34.281811
11105798	119.197698	34.268451
11106171	119.317652	34.28989
11106129	119.352373	34.58016
11106170	119.334111	34.313489
11105928	119.332858	34.348772
11100922	119.322307	34.38954
11102077	119.33852	34.319543
11120458	119.317652	34.321161
11105164	119.297092	34.325153
11100511	119.234496	34.382496
11105939	119.251238	34.360451
11100511	119.234496	34.382496
11105939	119.251238	34.360451
11105935	119.25202	34.370525
11101115	119.233681	34.432549
11121257	119.2338	34.433422
11101102	119.231976	34.432883
11121031	119.222902	34.402922
11120161	119.218663	34.542139
8303609	119.727188	34.400926
8303632	119.714455	34.40124
8303653	119.715492	34.402276
8303976	119.848383	34.434992
8304148	119.747003	34.899036
8304278	119.747152	34.928694
8304525	119.729351	34.876494
28303775	119.855967	34.40898
28304047	119.779482	34.365094
28304050	119.705845	34.34834
28304052	119.813845	34.367982
28304053	119.82462	34.363392
28304605	119.919105	34.393514
28304697	119.882622	34.389519
28304698	119.882484	34.3898
8303609	119.727188	34.400926
8303632	119.714455	34.40124
8303653	119.715492	34.402276
8303976	119.848383	34.434992
8304148	119.747003	34.899036
8304278	119.747152	34.928694
8304525	119.729351	34.876494
28303775	119.855967	34.40898
28304047	119.779482	34.365094
28303820	120.45	34.426468
28300100	120.46	34.411772
28303823	120.44	34.438653

Note: Well data and interpretations are available in the cited papers and the website of Department of Conservation, California (https://maps.conservation.ca.gov/doggr/wellfinder/#close).

REFERENCES CITED

Atwater, T.M., 1998, Plate tectonic history of southern California with emphasis on the western Transverse Ranges and northern Channel Islands, *in* Weigand, P.W., ed., Contributions to the Geology of the Northern Channel Islands, Southern California: American Association of Petroleum Geologists, Pacific Section, Miscellaneous Publication 45, p. 1–8, https://doi.org/10.32375/1998-MP45.1.

Bird, P., and Rosenstock, R.W., 1984, Kinematics of present crust and mantle flow in southern California: Geological Society of America Bulletin, v. 95, p. 946–957, https://doi.org/10.1130/0016-7606(1984)95<946:KOPCAM>2.0.CO;2.

Boyer, S.E., and Elliott, D., 1982, Thrust systems: American Association of Petroleum Geologists Bulletin, v. 66, p. 1196–1230.

Butler, R.W.H., 1987, Thrust sequences: Journal of the Geological Society [London], v. 144, p. 619–634, https://doi.org/10.1144/gsjgs.144.4.0619.

Corbett, E.J., and Johnson, C.E., 1982, The Santa Barbara, California, earthquake of 13 August 1978: Bulletin of the Seismological Society of America, v. 72, p. 2201–2226.

Crowell, J.C., 1979, The San Andreas fault system through time: Journal of the Geological Society [London], v. 136, p. 293–302, https://doi.org/10.1144/gsjgs.136.3.0293.

Darrow, A.C., and Sylvester, A.G., 1983, Activity of the Central Reach of the Santa Ynez Fault: Menlo Park, California, U.S. Geologic Survey Technical Report, 28 p.

Darrow, A.C., and Sylvester, A.G., 1984, Activity of the Central Reach of the Santa Ynez Fault: Continuation of Investigations: U.S. Geologic Survey Technical Report, Contract 21367, 18 p.

Davis, G.A., Burchfiel, B.C., 1973, Garlock fault: An intracontinental transform structure, Southern California Garlock fault: Geological Society of America Bulletin, v. 84, p. 1407–1422, https://doi.org/10.1130/0016-7606(1973)84<1407.

Davis, T.L., and Namson, J.S., 1998, USGS Cross Sections 3–8: http://davisnamson.com/index.htm (accessed 12 January 2018).

DeCelles, P.G., Robinson, D.M., Quade, J., Ojha, T.P., Garzione, C.N., Copeland, P., and Upreti, B.N., 2001, Stratigraphy, structure, and tectonic evolution of the Himalayan fold-thrust belt in western Nepal: Tectonics, v. 20, p. 487–509, https://doi.org/10.1029/2000TC001226.

Dibblee, T.W., 1982a, Regional geology of the Transverse Ranges Province of southern California, *in* Fife, D.L., and Minch, J.A., eds., Geology and Mineral Wealth of the California Transverse Ranges: Santa Ana, California, South Coast Geological Society, Inc., p. 7–26.

Dibblee, T.W., 1982b, Geology of the Santa Ynez–Topatopa Mountains, Southern California, *in* Fife, D.L., and Minch, J.H., eds., Geology and Mineral Wealth of the California Transverse Ranges: Santa Ana, California, South Coast Geological Society, Inc., p. 41–56.

Dibblee, T.W., 2002, Dibblee Geological Foundation: Geological Map Catalog (1–21, 24, 26, 27, 40–46, 53–55, 60, 186–189, 199–201, 254–259): https://www.sbnature.org/dibblee/ (accessed 20 July 2015).

Erslev, E.A., 1991, Trishear fault-propagation folding: Geology, v. 19, p. 617–620, https://doi.org/10.1130/0091-7613(1991)019<0617:TFPF>2.3.CO;2.

Farris, A.C., 2017, Quantifying Late Quaternary Deformation in the Santa Ynez Valley, Santa Barbara County, California [Master's thesis]: Long Beach, California, California State University, 150 p.

Groshong, R.H.J., 1994, Area balance, depth to detachment, and strain in extension: Tectonics, v. 13, p. 1488–1497, https://doi.org/10.1029/94TC02020.

Gurrola, L.D., Keller, E.A., Chen, J.H., Owen, L., and, Spencer, J.Q., 2014, Tectonic geomorphology of marine terraces; Santa Barbara fold belt, California: Geological Society of America Bulletin, v. 126, p. 219–233, https://doi.org/10.1130/B30211.1.

Hammond, W.C., Burgette, R.J., Johnson, K.M., and Blewitt, G., 2018, Uplift of the Western Transverse Ranges and Ventura area of Southern California: A four-technique geodetic study combining GPS, InSAR, leveling, and tide gauges: Journal of Geophysical Research–Solid Earth, v. 123, p. 836–858, https://doi.org/10.1002/2017JB014499.

Hauksson, E., Andrews, J., Plesch, A., Shaw, J.H., and Shelly, D.R., 2016, The 2015 Fillmore earthquake swarm and possible crustal deformation mechanisms near the bottom of the eastern Ventura Basin, California: Seismological Research Letters, v. 87, no. 4, p. 807–815, https://doi.org/10.1785/0220160020.

Hayes, G.P., Meyers, E.K., Dewey, J.W., Briggs, R.W., Earle, P.S., Benz, H.M., Smoczyk, G.M., Flamme, H.E., Barnhart, W.D., Gold, R.D., and Furlong, K.P., 2016, Tectonic Summaries of Magnitude 7 and Greater Earthquakes from 2000 to 2015: U.S. Geological Survey Open-File Report 2016–1192, 148 p., https://doi.org/10.3133/ofr20161192.

Hornafius, J.S., 1985, Neogene tectonic rotation of the Santa Ynez Range, Western Transverse Ranges, California, suggested by paleomagnetic investigation of the Monterey Formation: Journal of Geophysical Research, v. 90, p. 12503, https://doi.org/10.1029/JB090iB14p12503.

Hornafius, J.S., Kamerling, M., Terres, R., and Luyendyk, B., 1982, Differential tectonic rotation within the western Transverse Ranges: Geological Society of America Abstracts with Programs, v. 14, no. 4, p. 173–174.

Hornafius, J.S., Luyendyk, B.P., Terres, R.R., and Kamerling, M.J., 1986, Timing and extent of Neogene tectonic rotation in the western Transverse Ranges, California (USA): Geological Society of America Bulletin, v. 97, p. 1476–1487, https://doi.org/10.1130/0016-7606(1986)97<1476:TAEONT>2.0.CO;2.

Huang, W., Silver, L.T., and Kanamori, H., 1996, Evidence for possible horizontal faulting in southern California from earthquake mechanisms: Geology, v. 24, p. 123–126, https://doi.org/10.1130/0091-7613(1996)024<0123:EFPHFI>2.3.CO;2.

Hubbard, J., Shaw, J.H., Dolan, J.F., Pratt, T.L., McAuliffe, L.J., and Rockwell, T.K., 2014, Structure and seismic hazard of the Ventura Avenue anticline and Ventura fault, California: Prospect for large, multisegment ruptures in the Western Transverse Ranges: Bulletin of the Seismological Society of America, v. 104, p. 1070–1087, https://doi.org/10.1785/0120130125.

Hughes, A., Rood, D.H., Whittaker, A.C., Bell, R.E., Rockwell, T.K., Levy, Y., Wilcken, K.M., Corbett, L.B., Bierman, P.R., DeVecchio, D.E., Marshall, S.T., Gurrola, L.D., and Nicholson, C., 2018, Geomorphic evidence for the geometry and slip rate of a young, low-angle thrust fault: Implications for hazard assessment and fault interaction in complex tectonic environments: Earth and Planetary Science Letters, v. 504, p. 198–210, https://doi.org/10.1016/j.epsl.2018.10.003.

Jackson, P.A., 1981, Structural Evolution of the Carpinteria Basin, Western Transverse Ranges, California [Master's thesis]: Corvallis, Oregon, Oregon State University, 106 p.

Jordan, T.E., Allmendinger, R.W., Damanti, J.F., and Drake, R.E., 1993, Chronology of motion in a complete thrust belt: The Precordillera, 30–31°S: Andes Mountains: Journal of Geology, v. 101, p. 135–156.

Keller, E.A., and DeVecchio, D.E., 2013, Tectonic geomorphology of active folding and development of transverse drainages, *in* Shroder, J., ed., Treatise on Geomorphology: San Diego, California, Academic Press, p. 129–147, https://doi.org/10.1016/B978-0-12-374739-6.00088-9.

Leonard, M., 2010, Earthquake fault scaling: Self-consistent relating of rupture length, width, average displacement, and moment release: Bulletin of the Seismological Society of America, v. 100, p. 1971–1988, https://doi.org/10.1785/0120090189.

Ma, K.-F., Lee, C.-T., Tsai, Y.-B., Shin, T.-C., and Mori, J., 1999, The Chi-Chi, Taiwan, earthquake: Large surface displacements on an inland thrust fault: Eos (Washington, D.C.), v. 80, p. 605–611, https://doi.org/10.1029/99EO00405.

Marshall, S.T., Funning, G.J., and Owen, S.E., 2013, Fault slip rates and interseismic deformation in the Western Transverse Ranges, California: Journal of Geophysical Research–Solid Earth, v. 118, p. 4511–4534, https://doi.org/10.1002/jgrb.50312.

Marshall, S.T., Funning, G.J., Krueger, H.E., Owen, S.E., and Loveless, J.P., 2017, Mechanical models favor a ramp geometry for the Ventura–Pitas Point fault, California: Geophysical Research Letters, v. 44, no. 3, p. 1311–1319, https://doi.org/10.1002/2016GL072289.

McAuliffe, L.J., Dolan, J.F., Rhodes, E.J., Hubbard, J., Shaw, J.H., and Pratt, T.L., 2015, Paleoseismologic evidence for large-magnitude (Mw 7.5–8.0) earthquakes on the Ventura blind thrust fault: Implications for multifault ruptures in the Transverse Ranges of southern California: Geosphere, v. 11, p. 1629–1650, https://doi.org/10.1130/GES01123.1.

Miller, K.G., Kominz, A., Browning, J. V, Wright, J.D., and Mountain, G.S., 2005, The Phanerozoic record of sea level change: Science, v. 310, no. 5752, p. 1293–1298, https://doi.org/10.1126/science.1116412.

Morley, C.K., 1988, Out-of-sequence thrusts: Tectonics, v. 7, p. 539–561, https://doi.org/10.1029/TC007i003p00539.

Namson, J.S., and Davis, T., 1988, Structural transect of the western Transverse Ranges, California: Implications for lithospheric kinematics and seismic risk evaluation: Geology, v. 16, p. 675–679, https://doi.org/10.1130/0091-7613(1988)016<0675:STOTWT>2.3.CO;2.

Nazareth, J.J., and Hauksson, E., 2004, The seismogenic thickness of the southern California crust: Bulletin of the Seismological Society of America, v. 94, p. 940–960, https://doi.org/10.1785/0120020129.

Nicholson, C., Sorlien, C.C., Atwater, T., Crowell, J.C., and Luyendyk, B.P., 1994, Microplate capture, rotation of the Western Transverse Ranges, and initiation of the San Andreas transform as a low-angle fault system: Geology, v. 22, p. 491–495, https://doi.org/10.1130/0091-7613(1994)022<0491:MCROTW>2.3.CO;2.

Nicholson, C., Plesch, A., and Shaw, J.H., 2017, Community Fault Model Version 5.2: Updating and expanding the CFM 3D fault set and its associated fault database: 2017 Southern California Earthquake Center (SCEC) Annual Meeting, 10–13 September, 2017, poster 234.

Perea, H., Ucarkus, G., Driscoll, N.W., Kent, G.M., Levy, Y., and Rockwell, T.K., 2017, Holocene deformation events in the offshore Transverse Ranges (California, USA) constrained by new high-resolution geophysical data: Expanded abstract for the 8th International Union for Quaternary Research (INQUA) Meeting on Paleoseismology, Active Tectonics and Archeoseismology (PATA), New Zealand, 13–16 November 2017, p. 4.

Plesch, A., Shaw, J.H., Benson, C., Bryant, W.A., Carena, S., Cooke, M., Dolan, J., Fuis, G., Gath, E., Grant, L., Hauksson, E., Jordan, T., Kamerling, M., Legg, M., Lindvall, S., Magistrale, H., Nicholson, C., Niemi, N., Oskin, M., Perry, S., Planansky, G., Rockwell, T.K., Shearer, P., Sorlien, C., Süss, M.P., Suppe, J., Treiman, J., and Yeats, R.S., 2007, Community Fault Model (CFM) for southern California: Bulletin of the Seismological Society of America, v. 97, p. 1793–1802, https://doi.org/10.1785/0120050211.

Poblet, J., and Lisle, R.J., 2011, Kinematic evolution and structural styles of fold-and-thrust belts, *in* Poblet, J., and Lisle, R.J., eds., Kinematic Evolution and Structural Styles of Fold-and-Thrust Belts: Geological Society [London] Special Publication 349, p. 1–24, https://doi.org/10.1144/SP349.1.

Poblet, J., and McClay, K.R., 1996, Geometry and kinematics of single-layer detachment folds: American Association of Petroleum Geologists Bulletin, v. 80, p. 1085–1109, https://doi.org/10.1306/64ED8CA0-1724-11D7-8645000102C1865D.

Rockwell, T.K., 1983, Soil Chronology, Geology, and Neotectonics of the North Central Ventura Basin, California [Ph.D. thesis]: Santa Barbara, California, University of California, 424 p.

Rockwell, T.K., 1988, Neotectonics of the San Cayetano fault, Transverse Ranges, California: Geological Society of America Bulletin, v. 100, p. 500–513, https://doi.org/10.1130/0016-7606(1988)100<0500:NOTSCF>2.3.CO;2.

Rockwell, T.K., Keller, E.A., Clark, M.N., and Johnson D.L., 1984, Chronology and rates of faulting of Ventura River terraces, California: Geological Society of America Bulletin, v. 95, p. 1466–1474, https://doi.org/10.1130/0016-7606(1984)95<1466:CAROFO>2.0.CO;2.

Rockwell, T.K., Keller, E.A., and Dembroff, G.R., 1988, Quaternary rate of folding of the Ventura Avenue anticline, Western Transverse Ranges, southern California: Geological Society of America Bulletin, v. 100, p. 850–858, https://doi.org/10.1130/0016-7606(1988)100<0850:QROFOT>2.3.CO;2.

Rockwell, T.K., Nolan, J., Johnson, D.L., Patherson, R.H., 1992, Ages and deformation of marine terraces between Point Conception and Gaviota, Western Transverse Ranges California, *in* Fletcher, C.H., and Wehmiller, J.F., eds., Quaternary Coasts of the United States: Marine and Lacustrine Systems: Society for Sedimentary Geology (SEPM) Special Publication 48, p. 333–341.

Rockwell, T.K., Clark, K., Gamble, L., Oskin, M.E., Haaker, E.C., and Kennedy, G.L., 2016, Large Transverse Range earthquakes cause coastal upheaval near Ventura, Southern California: Bulletin of the Seismological Society of America, v. 106, p. 2706–2720, https://doi.org/10.1785/0120150378.

Rodgers, D.A., 1975, Deformation, Stress Accumulation, and Secondary Faulting in the Vicinity of the Transverse Ranges of Southern California [Ph.D. thesis]: Providence, Rhode Island, Brown University, 181 p.

Sarna-Wojcicki, A.M., and Yerkes, R.F., 1982, Comment on article by R.S. Yeats on "Low-shake faults of the Ventura Basin, California," *in* Cooper, J.D., compiler, Neotectonics in Southern California, 78th Annual Meeting Guidebook: Anaheim, California, Cordilleran Section, Geological Society of America, p. 17–19.

Schlueter, J.C., 1976, Geology of the Upper Ojai–Timber Canyon Area, Ventura County, California [M.S. thesis]: Athens, Ohio University, 76 p.

Schwartz, D., 2018, Large coherent block versus microplate rotation of the Western Transverse Ranges: A fresh look at paleomagnetic constraints [M.S. thesis]: San Diego, California, University of California–San Diego, 37 p.

Shaw, J.H., and Suppe, J., 1994, Active faulting and growth folding in the eastern Santa Barbara Channel, California: Geological Society of America Bulletin, v. 106, p. 607–626, https://doi.org/10.1130/0016-7606(1994)106<0607:AFAGFI>2.3.CO;2.

Shaw, J.H., Connors, C.D., and Suppe, J., 2005, Seismic Interpretation of Contractional Fault-Related Folds: An AAPG Seismic Atlas: American Association of Petroleum Geologists Studies in Geology 53, 156 p.

Smit, J.H.W., Brun, J.P., and Sokoutis, D., 2003, Deformation of brittle-ductile thrust wedges in experiments and nature: Journal of Geophysical Research, v. 108, p. 2480, https://doi.org/10.1029/2002JB002190.

Sorlien, C.C., and Nicholson, C., 2015, Post–1 Ma Deformation History of the Pitas Point–North Channel–Red Mountain Fault System and Associated Folds in Santa Barbara Channel, California: U.S. Geological Survey National Earthquake Hazards Reduction Program Final Report, Award G14AP00012, 24 p.

Storti, F., Salvini, F., and McClay, K.R., 1997, Fault-related folding in sandbox analogue models of thrust wedges: Journal of Structural Geology, v. 19, p. 583–602, https://doi.org/10.1016/S0191-8141(97)83029-5.

Suppe, J., 1983, Geometry and kinematics of fault- bend folding: American Journal of Science, v. 283, p. 684–721, https://doi.org/10.2475/ajs.283.7.684.

Suppe, J., and Medwedeff, D.A., 1990, Geometry and kinematics of fault-propagation folding: Eclogae Geologicae Helvetiae, v. 454, p. 409–454, https://doi.org/10.5169/seals-166595.

Wells, D.L., and Coppersmith, K.J., 1994, New empirical relationships among magnitude, rupture length, rupture area and surface displacement: Bulletin of the Seismological Society of America, v. 84, p. 974–1002.

Wiltschko, D.V., and Dorr, J.A., 1983, Timing of deformation in Overthrust belt and foreland of Idaho, Wyoming, and Utah: American Association of Petroleum Geologists Bulletin, v. 67, p. 1304–1322, https://doi.org/10.1306/03B5B740-16D1-11D7-8645000102C1865D.

Yeats, R.S., 1983, Large-scale Quaternary detachments in Ventura Basin, southern California: Journal of Geophysical Research, v. 88, p. 569–583, https://doi.org/10.1029/JB088iB01p00569.

Yeats, R.S., and Rockwell, T.K., 1991, Quaternary geology of the Ventura and Los Angeles Basins, California, *in* Morrison, R.B., ed., Quaternary Nonglacial Geology: Conterminous U.S.: Boulder, Colorado, Geological Society of America, The Geology of North America, v. K-2, p. 185–189.

Yeats, R.S., Huftile, G.J., and Grigsby, F.B., 1988, Oak Ridge fault, Ventura fold belt, and the Sisar décollement, Ventura basin: California Geology, v. 16, p. 1112–1116, https://doi.org/10.1130/0091-7613(1988)016<1112:ORFVFB>2.3.CO;2.

Yerkes, R.F., and Lee, W.H.K., 1987, Late Quaternary deformation in the Western Transverse Ranges, *in* Recent Reverse Faulting in the Transverse Ranges, California: U.S. Geological Survey Professional Paper 1339, p. 71–82.

MANUSCRIPT RECEIVED 8 JULY 2019
REVISED MANUSCRIPT RECEIVED 25 AUGUST 2019
MANUSCRIPT ACCEPTED 15 OCTOBER 2019